Impulse Transfer during Sand Impact with a Cellular Structure

Ryan L. Holloman[1], Vikram Deshpande[*], Haydn N.G. Wadley

Department of Materials Science & Engineering
University of Virginia, Charlottesville, VA 22903
[*]Engineering Department
University of Cambridge, Trumpington Street, Cambridge, UK

Abstract

Compressible cellular metal sandwich structures made from a 3D assembly of square cross section 6061 T6 aluminum alloy tubes, and face sheets of the same alloy have been attached to a vertical pendulum and impacted by synthetic wet sand with an incident velocity of ~300 ms^{-1}. The transmitted impulse of samples with thick (relatively rigid) and thin face sheets are compared to that transferred by an incompressible solid aluminum test block of the same dimensions. A discrete particle-based simulation method was used to simulate the experiments and to investigate the soil particle – structure interaction with the cellular structures. The simulated results agreed very well with experimental data; both showed that the impulse transferred to cellular structures with a 22 MPa core strength was 10-15% less than that transferred to a solid block of similar dimensions. However, the simulations reveal that the some of this apparent mitigation resulted from a subtle sand interaction between the bottom of the test structure and the sand box used for the tests. When this sand box effect was eliminated in the simulations, a small impulse reduction from cellular structures with thin face sheets was still observed. However, this was found to be a result of dynamic deflection of the edges of the front face sheet. When this effect was eliminated (by the use of a rigid front face), the simulations showed a small (5%) impulse reduction occurred for cellular structure whose compressive strength was much less than the pressure applied by the sand. This was a consequence of rapid core compression which increased the travel distance (and lateral spreading) of late arriving sand during the sand loading process. Weak cellular structures, that suffered significant crushing, also reduce the impulse transfer rate.

Key words: 6061 Aluminum, Blast loads, Cellular structures, Discrete particles, Sand ejecta

[1] Corresponding Author
rlh5v@virginia.edu
+01 3039466325

Introduction

Compressible cellular materials are widely used for protecting structures from impulsive loads created by impacts[1, 2]. For example, light, low compressive strength polymeric foams are used as a part of packaging systems to protect fragile objects during transport, and in helmets as a key component of a strategy to reduce the risk of traumatic brain injury[3]. In each application, the stress applied to the protected object is controlled by the compressive strength of the cellular material[4]. When these cellular materials are integrated into structures with strong faces, localized (impact) loads are spatially and temporally dispersed, further reducing the risk of damage or injury[5]. The emergence of compression resistant, metallic cellular structures[4 6 7] led to an interest in the extension of these concepts to the protection of structures from high intensity impulsive loads caused by nearby explosions[8, 9, 10, 11, 12.]

Several studies have investigated impulse transfer by cellular structures, configured as the cores of sandwich panels, during underwater impulsive loading[13, 14, 15]. The impact of one of the face sheets by a water propagated shock was shown to result in a transfer of momentum to the face sheet that was governed by a fluid structure interaction (FSI) resulting from shock reflection at the face sheet - water interface[16, 17 ,18]. For (rigidly supported) face sheets that remained stationary during shock reflection, the momentum transferred to a structure was twice the incident value. However, the reflection coefficient (and transferred impulse) was reduced when the face sheet was allowed to move during the shock reflection process. This could be achieved by decreasing the mass per unit area of the impacted face sheet, and the ratio of the core compressive strength to shock pressure. In well-designed structures, the ensuing motion of the impacted face sheet was arrested by reaction forces activated by core compression and face sheet and core stretching as the sandwich panel suffered out of plane deflection. These forces could be controlled by the cellular core topology, its relative density and by the mechanical properties of the material used to fabricate it. The use of light (thin) front face sheets, and weak cores whose dynamic crush strength was less than the pressure applied by the shock front, enabled significant (up to 50%) reductions in impulse transfer to the protected structure[19, 20, 21]. However, when the shock pressure to core strength ratio was too high, complete core densification was predicted. The ensuing “slap” event (as the front face sheet and densified core were accelerated against the

rear of the structure), could then lead to impulse magnification; especially if the shock loading was in-phase over a large area of the face sheet (planar shock fronts impinging flat face sheets at zero obliquity)[11].

Underwater experiments utilizing instrumented Hopkinson pressure (or Kolsky) bars attached to back supported, impulsively loaded structures have been used to study pressure (and impulse) transmission during quasi-planar underwater shock front loading of cellular core sandwich structures [22, 23]. Many core topologies for these studies were fabricated from corrosion resistant stainless steels[24, 25, 26] including honeycombs[23], corrugated structures[22], and lattices with a pyramidal truss arrangement[27]. All were able to significantly reduce the transferred impulse and pressure. These studies showed that significant reductions in transmitted pressure (and momentum) could be realized when weak core systems were utilized. They also showed that when the shock pressure was sufficient to completely collapse (densify) the cellular structure, slap of the front face sheet against the densified core did cause a rise in pressure and impulse transfer, but this was much less than model predictions.

Efforts to extend the cellular structures approach to edge restrained test configurations revealed the important role of the core in supporting panel stretching[17]. Since the pyramidal lattice offered little in-plane stretch resistance, square or triangular honeycomb cores[28] were preferred, but were more difficult to fabricate. Related studies have also investigated the response of edge clamped sandwich panels to explosive shock loading in air, and led to the experimental discovery of significant reductions of back face sheet deflection compared to equivalent monolithic plates[29, 28], even though the FSI effect was weaker in air[30, 31].

Recently, experimental work has begun to characterize momentum and pressure transfer during the impact of explosively accelerated soil against sandwich structures with compressible cores[32, 33, 34, 35, 36, 37]. Discrete particle based simulation approaches have also been used to model the transfer of momentum from high explosive reaction products to air and soil particles, and from these to model test structures[38]. This same model approach was later used to investigate soil interactions with an edge restrained aluminum sandwich structure[39]. These studies showed that significant reductions in back face panel deflection could occur when a solid plate was

redistributed to form a strong core sandwich panel, consistent with other studies[35]. Sand impact with aluminum sandwich panels also revealed the existence of a strong coupling between local compressions of the core, dynamic deflection of the impacted face sheet and the local impulse transfer mechanism. Local surface concavities more strongly reflected the sand particles, resulting in a locally higher momentum transfer to that region. The higher local loading of the sandwich by sand particle reflection during dynamic evolution of the panel's surface topology, amplified local core crushing and face sheet stretching leading to fracture, and focused attention upon the need for a deeper understanding of the soil structure interaction (SSI) effect.

The impact of sand particle columns against rigid surfaces at zero obliquity has been experimentally investigated by Park et al[40]. Using wet and dry sand column's with impact velocities up to 100 ms^{-1}, they found that the pressure applied by the sand was hydrodynamic and approximately equal to ρv^2 (where ρ was the sand column density and v its incident velocity); the stagnation pressure of the sand. This inertial loading then transferred its incident momentum to the test structure with very little amplification (less than 10%) from sand particle reflection. This observation has been recently confirmed for explosively accelerated wet sand impact (at a velocity of ~300 ms^{-1}) against a solid aluminum test block[41]. Coupled discrete particle/finite element simulations of the impact of sand columns against back supported cellular structures by Lui et al.[42] identified the existence of a small (<10%) reduced impulse transfer regime when the compressive strength of the core was less than the stagnation pressure applied by the sand, but not so small that face sheet slap occurred. These simulations also indicated that the effect was sensitive to the axial density gradient and length of the sand column, and the thickness of the core.

Here, a recently proposed 3D cellular structure, made from square cross section Al 6061-T6 tubes,[43] is utilized to experimentally investigate the impulse and pressure transfer mechanisms to a back supported cellular core sandwich structure impacted by soil. The quasi-static[43] and dynamic compression[44] of the 3D tube core structure has been previously examined in detail, and the structures response was shown to be rate independent for the compression rates of interest. We investigate the compressive response of this structure when attached to both thin and thick impact face sheets, as it is subjected to approximately planar loading by explosively

accelerated wet silica glass micro-spheres. The experiments were conducted in the same vertical pendulum recently used to study the sand-structure interaction with a back supported solid block[41]. Differences in the response of the cellular and solid block structures could therefore be observed and quantified. The same discrete particle based simulation used to analyze solid block interactions with sand is then used to interpret the experiments, and to more fully investigate the soil-cellular structure interaction process.

2. Test sample fabrication

The study utilized three test samples shown schematically in Figure 1. The solid block used in the previous study of the soil – structure interaction is shown in Figure 1(a). The cellular structures were manufactured by first laying down a co-linear layer of 6061 aluminum alloy square tubes each spaced a tube width apart. A second, similarly spaced layer was then orthogonally placed on the first, and the assembly sequence repeated to create a $[0^o/90^o]_2$ structure. The 3D topology was assembled from the 2D array by inserting identical tubes in the out-of-plane (vertical) void space between the cross-ply oriented tubes. The 3D core was attached to either 12.7 mm or 4.7 mm thick front face sheets to create the two other sample types tested, Figure 1(b) and (c). All the structures were attached to 4.7 mm thick back face sheet with a pre-drilled set of holes that permitted attachment to the test rig. The out-of-plane tubes in the 3D cellular structure were notched to facilitate complete fluid penetration during a subsequent dip brazing operation used to bond the various components of the test structure. After brazing the structure was heat treated to the T6 (peak aged) condition. A full description of the sample fabrication and mechanical properties of the cellular structure has been previously reported[43].

The geometry and mass of the 3D test structures investigated here are summarized in Table 1, and Figure 1. The core of the sandwich structures occupied a volume of $3.14x10^{-3}\ m^3$ while the aluminum in the 3D core occupied a volume of $6.3x10^{-4}m^3$ resulting in a core relative density $\bar{\rho} = 20.1\%$. The solid aluminum block, Figure 1(a), had the same volumetric dimensions as the cellular core structure. Both structures in 1(b) and 1(c) had identical cores; however, the different thickness front face sheets led to the thickness of the three

structures to vary, as shown in Figure 1. The core compressive strength was 21.8 MPa and independent of strain rate [43, 44].

3. Blast Loading Test Procedures

The cellular structures were loaded by explosively accelerated wet synthetic sand in the same vertical impulse loading facility used to study impulse transfer by the same sand to solid block samples[41]. Figure 2 shows a schematic representation of the vertical impulse test apparatus. The reader is referred to Holloman et al.[41] for a detailed description. The separation distance, δ, between the front face of the three test structures and the outside surface of the top plate of the steel sand box enclosure (Figure 2) varied during this study as a result of the different test structure thicknesses, Figure 1. The gap, δ, for the solid block was 8.1 mm; 9.7 mm for the thin face sheet cellular structure, and 1.8 mm for the thick face sheet cellular structure. Figure 2 shows the test geometry for a thin face sheet cellular structure.

A 50.4 mm thick layer of synthetic sand (consisting of 150-200 μm diameter amorphous silica particles) with 80% water saturation, was placed on top of a 300 g planar layer of explosive about 3 mm in thickness that rested on a polymer foam foundation. This charge was detonated using an array of five detonators connected by 5, 10 g C4 explosive boosters, to create a planar impulsive load that accelerated the wet sand towards the test structure at a velocity of ~300 ms^{-1}. The sand that passed through a square aperture in a solid steel plate on top of the sand enclosing box then impacted the lower surface of each test structure. The standoff distance between the top of the explosive sheet and the bottom of the test structure was varied between 14 and 40 cm to change the impulse applied by the sand. The samples were attached to an apparatus that could be used either as a vertical pendulum or to measure the pressure waveform applied by the sand. In the latter mode, the pressure was determined using strain gauges located at the four pressure bar locations shown in Figure 2.

4. Experimental results

4.1 Vertical pendulum mode

The impulse transmitted by the sand to the cellular core sandwich structures were first deduced from the pendulum jump height and mass are summarized in Table 2 and compared with analogous data for the solid block sample. The impulse transferred to the solid aluminum block and cellular structure with a thick face sheet is shown as a function of standoff distance in Figure 3(a). The impulse applied to the solid block was experimentally observed to decrease from approximately 14 kPa·s, for a standoff distance of 14 cm, to approximately 8 kPa·s at a standoff distance of 40 cm. The impulse acquired by the cellular structure with a thick face sheet was less than that of the solid block; it decreased from approximately 12.5 kPa·s at a standoff distance of 14 cm, to approximately 8 kPa·s at a standoff distance of 40 cm. The error bars shown with the data were estimated from the uncertainty in pendulum height during the exposure time of a high speed video image and from estimates of the parallax error. The impulse transferred to the solid block decreased linearly with standoff distance, and had a slope $=-0.20\ kPa \cdot s \cdot cm^{-1}$. The impulse transferred to the thick front face covered cellular structure also decreased linearly with standoff distance, but with a slightly smaller slope $=-0.16\ kPa \cdot s \cdot cm^{-1}$. The impulse of the thin faced sandwich structure decreased from approximately 11.5 kPa·s at a standoff distance of 14 cm, to approximately 8 kPa·s at 40 cm, Figure 3(c). The impulse of the thin faced sandwich structure decreased linearly with standoff distance with a slope of $-0.14\ kPa \cdot s \cdot cm^{-1}$.

4.2 Hopkinson pressure bar mode

The pressure-time responses for the thin face cellular structures (measured at the strain gauge locations on the four Hopkinson pressure bars) are shown in Figure 4 (solid black lines) for each standoff distance. Time *t=0,* corresponded to detonation of the test charge. All the pressure-time signals exhibited an initially sharp rise to a peak pressure that decreased with increasing standoff distance. Following the initial pressure peak, a period of declining pressure was observed before the first reflected signal arrived at the strain gauge locations (shown on the figures). Its slope decreased with standoff distance, and at the largest standoff distance, the slope of this region was almost flat (a plateau), Figure 4(d). There was an abrupt drop in pressure

corresponding to the arrival of the first (sign converted) reflected signal at the sensor location, followed by elastic reverberations of the Hopkinson bars.

The pressure-time curves shown in Figure 4(a)-(d) were integrated to calculate the impulse-time curves shown in Figure 5 (solid black lines). The time at which the first distal reflection and the second reflected signals reached the sensors on the Hopkinson bars ($558\ \mu s$ and $748\ \mu s$ respectively) are shown for each standoff distance. The first refection was sign converted upon reflection from the top of the bar and its arrival caused a sharp drop in pressure, and inflection in the impulse–time response. The second reflection had under gone two sign reversals, and was in phase with the continuing direct signal. Its arrival therefore caused the impulse to again start rising.

The peak pressures for each standoff distance are summarized in Table 3, and plotted against standoff distance in Figure 6(a). Table 3 and Figure 6(a) also shows that the peak pressures recorded for the solid aluminum block were greater than those for the cellular structure at the same standoff distance. The pressure applied to the solid block was observed to decrease from approximately 28 MPa at a standoff distance of 14 cm, to approximately 10 MPa at a standoff distance of 40 cm. At the shortest standoff distance of 14 cm, the initial peak pressure transmitted by the cellular structure was 19.4 MPa. This fell with increase in standoff distance to 7.2 MPa at a standoff distance of 40 cm. The pressure applied by the solid block decreased linearly with standoff distance with a slope $=-0.7\ MPa \cdot cm^{-1}$. The pressure applied by the thin front face cellular structure also decreased linearly with standoff distance, but with a slope = $-0.5\ MPa \cdot cm^{-1}$. The cellular structures crush strength (21.8 MPa) has been previously reported[43] and is shown on Figure 6(a).

Integration of the pressure data acquired up to the arrival of the first bar reflection, Figure 5, indicated that a substantial fraction of the full impulse was acquired during the first $558\ \mu s$ of sand impact. The initial slope of pressure time response gives an estimate of the impulse transfer rate, $\dot{I}$. Using the data shown in Figure 5, $\dot{I}$ = 18.8 MPa at a 14 cm standoff and fell to 6.9 MPa at a 40 cm standoff distance; consistent with the average pressure during the first $558\ \mu s$ pressure measured with the Hopkinson bars, Table 3. The impulse rate for the comparable solid

aluminum block is also presented in Table 3 and exceeded that of the cellular structure. The impulse obtained by integrating the pressure waveform for 558 μs after the first direct arrival is summarized in Figure 6(c). The measured impulse transmitted by the cellular structure was 2-3 kPa·s lower than that transmitted by the solid block, Figure 3(c).

The test samples were sectioned and photographed to reveal their mid-plane deformation, Figure 7 and 8. The collapse mechanisms shown in Figures 7 and 8 are consistent with those found during the previous quasi-static[43] and dynamic[44] studies. Core crushing was initiated by the onset of buckling of the tubes oriented in the through thickness direction, and was nucleated at the notches in the out of plane tubes. The vertical side walls of the in-plane tubes then began to buckle and constrained the amplitude of the vertical tube buckling. This led to repeated folding of the vertical tubes and a plateau-like stress-plastic strain response. The change in core thickness was used to calculate the core plastic strain caused by sand impact with both the thick and thin front faced cellular structures. These results are shown as a function of incident impulse (taken to be that transferred to the solid bock samples at each standoff distance) for both sample types in Figures 9(a) and (b). The core strains of the thin face samples were approximately the same as those of samples with a thick front face sheet. Examination of Figures 7 and 8 show that the sides of the face sheets, especially for the most severely loaded samples, had been dent upwards by the sand impact, and the impacted surface therefore acquired a slightly convex shape (when viewed from below).

The difference in impulse transferred by the solid block and cellular structures has been divided by the impulse transferred by the solid block and is plotted against incident impulse transferred to the solid block in Figures 9(c) and (d) for samples with thick and thin faces. It can be seen that the reduction in impulse transferred by the cellular structures increased with incident impulse (i.e. with reduction in standoff distance), and that samples with thinner face sheets suffered a large change.

5. Numerical simulations

The commercial IMPETUS Afea Solver[45] was used to simulate the experiments conducted with the vertical impulse test apparatus. A detailed description of its implementation to analyze the vertical impulse test facility and earlier experiments with the solid block sample can be found in Holloman et al.[41]. Briefly, the code uses particle based methods to simulate the detonation of an explosive from a single detonation location, and track momentum transfer from high pressure explosive reaction products to surrounding air and sand particles. These particles then interact with each other, and eventually contact the test structure and sample surfaces, applying contact forces to them. The resulting deformation of the test structure and samples is then modeled using a finite element method[46].

A convergence study was conducted to determine the optimum number of discrete particles. From this study convergence was reached with 2,000,000 discrete particles. These particles were distributed by the IMPETUS Afea Solver as 45,595 air particles, 1,941,610 soil particles, and 12,795 high-energy explosive reaction product particles based on prior work by Borvik et al.[38]

5.1 The cellular structure model

The geometry and relative density of the modeled cellular specimens was the same as that reported in Table 1. Following usual practice[47, 48, 49], small imperfections were incorporated in the models to account for manufacturing defects (such as tube misalignment and tube wall thickness variability) in the tested specimens that tripped tube wall buckling under compressive loading. The imperfections were introduced as a displacement to each tube wall with a spatial distribution corresponding to the lowest order buckling eigenmode. For all the modeled structures, the first order eigenmode amplitude was set at 0.1 times the tube wall thickness.

5.2 Material properties

The experimentally determined Cauchy stress-true strain response of the Al 6061-T6 alloy used to make the test specimens was presented in Holloman et al.[44] The uniaxial Cauchy

stress, σ, versus true strain, ε, relation for an elastic-plastic material under uniaxial straining can be written:

$$\varepsilon = \varepsilon_e + \varepsilon_p = \frac{\sigma}{E} + \varepsilon_p \quad (1)$$

where ε_e and ε_p are the elastic and plastic components of strain and E is Young's modulus. The true stress versus plastic strain curve was tabulated and used to determine an isotropic strain hardening relation needed for FE simulations. The transition from elastic to plastic behavior was set at a Cauchy stress of 230.7 MPa. The hardening tabulation was implemented in the IMPETUS Afea Solver using the general piecewise linear hardening constitutive model with optional thermal softening and strain rate hardening. The yield stress of this model is defined in the form:

$$\sigma_y = f(\epsilon_{eff})(1 - (\frac{T - T_0}{T_m - T_0})^m)(1 + \frac{\dot{\epsilon}_{eff}}{\dot{\epsilon}_0})^c \quad (2)$$

where $f(\epsilon_{eff})$ is the piecewise linear hardening function of the effective deviatoric strain, which was obtained from the hardening curve behavior. The thermal softening component was defined by the current temperature, T, the reference temperature, T_0, the melting temperature, T_m, and the thermal softening parameter, m. The strain rate hardening component of Eq (2) was defined by a reference strain rate, $\dot{\epsilon}_0$, and a strain rate hardening parameter, c. The coefficients used in conjunction with Equation 2 to model the material are given in prior work[44]. We note that the thermal softening and strain rate hardening components made a negligible contribution to the flow stress. This was primarily defined by the piecewise linear hardening function $f(\epsilon_{eff})$ modeled using a von Mises yield criterion with isotropic hardening.

To account for softening resulting from tube wall fracture on the tensile side of severely buckled tubes, the Cockcroft-Latham failure criterion[50] was implemented for all the simulations. In this approach, failure is defined to occur when a damage parameter, D, reaches unity. The damage parameter was calculated as:

$$D = \frac{1}{W_c}\int_0^{\epsilon_{eff}} \max(0, \sigma_1)\, d\epsilon_{eff} \quad (3)$$

where σ_1 is the first principle stress. The critical damage parameter, W_c =85 MPa was obtained by fitting the simulated measured stress-strain response of a single laterally compressed tube tested in the prior work[44]. The general node splitting feature in the IMPETUS code was turned

on. This feature allowed the damage variable to evolve without change to the constitutive response of the Al 6061-T6 alloy until D=1. At that instant, the Al6061-T6 alloy was assumed to have failed and nodes of the elements where this failure had occurred were split.

The FE model was constructed from 7,104 cubic and 19,608 linear hexahedra elements with 246,216 nodes. The Hopkinson bars and all connecting parts were modeled with a coarse mesh since material failure was not seen experimentally. The solid test block was modeled with a finer mesh since some local deformation (thought to be associated with sand fingers) was observed experimentally. The solid block was constructed from 16,944 8-node 3rd-order linear hexahedra elements. The cellular structure sample with a thin front face sheet was constructed with 19.278 8-node 3rd-order linear hexahedra elements and the cellular structure sample with a thick front face was constructed from 15,568 8-node 3rd-order linear hexahedra elements. A mesh sensitivity study was performed for all three sample types to confirm solution convergence with this level of discretization.

6. Simulation Results and Discussion

6.1 Comparisons with experiments

The IMPETUS code enables a direct computation of the momentum incident upon the front face of a test structure. This feature was used to calculate the impulse transferred to the solid Al block and to the cellular samples with thick and thin impact faces. The simulated impulse transferred to the solid block and thick front cellular samples is shown as a function of standoff distance in Figure 3(b). Similar data for the thin faced sample is shown in Figure 3(d). The magnitudes of the simulated impulses for both the solid and cellular structures were in good agreement with those measured with the vertical pendulum, and declined with increasing standoff distance. Within the experimental range of standoff distances, the impulse transferred by the cellular structures was usually less than that transferred by the solid block, and the difference was slightly large for the thin faced samples, Figures 3(a) and 3(c). To more clearly establish the trends with standoff distance, additional simulations were performed at shorter and longer standoff distances, and this data is shown on Figures 3(b) and 3(d). These simulations show that at large standoff distances (low incident impulse levels), where no core compression occurs,

there is no difference in the impulse transferred to the solid and cellular structures. Decreasing the standoff distance below 14 cm confirms that substantial impulse mitigation continues to occur, especially for the cellular structure with the thinner impact face.

Additional simulations were conducted to determine the pressure versus time history at the Hopkinson bar sensor locations. The average of the signals recorded on the four bars is shown in Figure 4 for the cellular structures with a thin impact face. Before the arrival of the first reflection, the simulated and measured pressure histories (and especially the peak pressures) are in good agreement. Past the first reflected wave, reverberations within the Hopkinson bar dominated the response, and it was difficult to accurately simulate the response in part because of poorly known reflection coefficients and dissipation processes of the bars. The most notable discrepancy between the measured and simulated pressure waveforms was the time at which the pressure began to rise. This occurred earlier in the simulations, and was most noticeable at longer standoff distances. This phenomenon was observed in the earlier study of the solid block response and was attributed to the arrival of (anomalous) high velocity spalled sand[41], due to insufficient momentum transfer from sand to air particles. Figure 6(b) provides a summary of the simulated peak pressure predictions for the solid block and thin front face cellular structure. The simulated peak pressure was slightly higher than that observed experimentally as a consequence of the higher sand front velocity.

The impulse was obtained by integration of the simulated pressure waveforms, and is shown in Figure 5 for the cellular structures with a thin front face. Again, relatively good agreement with measured results was obtained up to the first reflected wave arrival. Following the first (sign reversed) reflected wave arrival, the impulse plateaued or decreased, before again rising when the twice reflected, non-sign reversed signal arrived ($190\ \mu s$) after the first reflected arrival. Reverberation and dissipation within the bars was not as well modeled by the simulation methodology, but even so, the general trend of rising impulse towards a final value was evident in the simulated data, Figure 5. The impulse obtained by integration (for 558 μs) of the measured and simulated pressure waveforms is plotted versus standoff distance in Figure 6(d). By extending the simulations to larger standoff distances than those used in experiments, it can be seen that the reduction in early stage impulse decreased to zero as the standoff distance was

increased. The simulated change in impulse versus incident impulse for samples with a thick impact face is shown in Figure 9(c) and for those with a thin impact face in Figure 9(d). The simulated results again agree well with both sets of measurements.

The effective plastic strain distribution and overall deformation of the two sets of cellular test structures are shown in Figures 7 and 8. The buckling collapse of the core and the convex deflection of the thin face sheet samples are well predicted. However, the simulations overestimated the convexity acquired by the impact face of the thick face samples. This may be a result of the use of a single (central) detonator location in the simulations rather than the five in the experiment which would have produced a slightly more spatially uniform impulse distribution. The plastic compressive strain of the cores is shown versus incident impulse in Figure 9(a) and (b) for both types of cellular structure. It can be seen that there was very good agreement between the measured and simulated core strains.

6.2 Sand impact visualization

A sequence of sand (brown) and detonation product (burgundy) particle position snap shots for the solid block, thin faced, and thick faced cellular structures are shown for the 14 and 40 cm standoff distance tests in Figures 10 and 11. Twenty spherical virtual particle “monitors” each with a radius of 0.508 cm were positioned 2.5 cm below the lower surface of the solid block, and distributed in a line across the full mid-plane of the specimen, Figures 10(a) and 11(a). The monitors (not shown in the simulations) were positioned at the same positions within the box lid aperture opening for the cellular structure simulations. This resulted in the monitors being initially located 2.7 cm below the thin face specimen front face sheet and 1.9 cm below the thick face sheet sample. In all three cases, it can be seen that the explosively accelerated sand above the explosive traveled in (predominantly) the upwards direction. A small lateral acceleration was also imparted to the synthetic sand layer causing it to widen over time (and distance of propagation). The upward accelerated sand acquired a range of velocities as a result of loading by a combination of shock reflection and the push from the expanding detonation products. It therefore increased in thickness with distance travelled.

At the 14 cm standoff distance, the fastest sand began to load the samples at ~0.24 ms after detonation, Figure 10(b), and at about 0.6 ms for the 40 cm standoff distance, Figures 11(a) and (b). The test samples then began to suffer an upwards displacement as the solid block and Hopkinson bars were elastically compressed, and the cellular structures began to plastically crush. The upward motion of the sand that impacted the solid block was arrested and displaced laterally across the flat surface. As it reached the sides of the sample it was forced to propagate through the narrow gap between the sand box lid and the bottom of the sample. Initially, sand accumulated just below the sample since the sand particle arrival rate exceeded that of escape through the gap. The upward motion of the impacted surface of the samples increased the gap with the lid and eventually enabled more rapid sand escape. However, sand particle impact with the underside of the lid also caused it to suffer an initially upward displacement during the experiment. The gap separation was controlled by vertical displacement of the sample (due to compression and extension of the samples and test structure) and oscillation of the sand box lid which are shown in Figure 12 for the three topologies at a 14 cm standoff distance. The evolution of the position of the lid and impacted surface of the samples is shown in Figure 13(a) and the gap separation in Figure 13(b). The gaps for the cellular samples were wider than those of the solid because of plastic core compression. The sides of the face sheet of the thin faced cellular sample were also more significantly bent by the escaping sand than the sample with the thick front face, Figure 12, and so their gaps with the sand box lid surface were larger throughout most of the sand loading process.

The effect of increasing the standoff distance can be seen by comparing Figures 10 and 11. The sand layer was more significantly stretched as the standoff distance increased. This decreased the sand arrival rate, and in turn decreased the pressure on the test structure and its initial upward deflection, and also resulted in less plastic core compression for the two cellular structures, Figure 14. As a result of these off-setting effects, substantial sand accumulated beneath the three sample types, but was again more rapidly relieved in the thin front face structure by opening of the gap, Figure 15.

More insight into the sand loading process can be gained by examining the monitor deduced sand velocity – time profiles, Figures 16(a) and 17(a). Apart from small random

deviations and the slight difference in distance to the test sample, these were identical for the three sample types. At a 14 cm standoff distance the sand particles reached a peak velocity of approximately 400 ms^{-1} at 0.2 ms after detonation. Figure 10(a-b) shows that this highest velocity was associated with spalled sand traveling at the sand front's leading edge. The most significant difference in the sand velocity of the three topologies was observed at ~0.4 ms after detonation when the main sand layer arrived. The monitors positioned below both cellular structures had a sand velocity of approximately 200 ms^{-1} at this time, whereas the solid block sand velocity was substantially lower (approximately100 ms^{-1}), consistent with extra accumulated sand that had stagnated against the sample. This difference is highlighted in Figure 10(d) where the sand contacting the solid block had limited opportunities to escape while the core crushing and the face sheet edge deformation allowed the sand to more easily flow past the steel box top. When the standoff distance was increased, the sand velocity exhibited less deviation between topologies, Figure 17(a). This is visually apparent in Figures 11(c and d) where less core crushing occurred, and the cellular structures acted more like the incompressible solid block.

The sand density – time profiles at the monitors differed more significantly than the velocity – time outputs for the three topologies. At a 14 cm standoff distance the sand density at the monitors below the cellular structures reached a higher value (1400-1600 kgm^{-3}) than the solid block during the time (0.3-0.5 ms) of core crushing, Figure 16(b). After reaching a maximum, the sand density fell most rapidly for the thin faced cellular structure. The drop in density is visually apparent in Figures 10(c and d), and corresponded with rapid sand flow from the steel box as the cores crushed and the gap, δ, increased. The incompressible solid block forced much of the sand to stagnate against the impact face. A similar effect occurred for the thick front face sheet sample which suffered smaller plastic compression than the sample with the thin face sheet. At the 40 cm standoff distance, the density – time outputs from the monitors exhibited similar trends, Figure 17(b). Once again, this was directly controlled by the separation distance with the sand box structure. The slower drop in sand density for the thin face sheet cellular structure at the 40 cm standoff distance (compared to that at 14 cm) was due to less core crushing.

The hydrodynamic pressure (P_h) applied by the sand particles, could be calculated from the numerically measured sand density, ρ, and velocity, v, with the spherical monitors using:

$$P_h = \rho v^2 \tag{4}$$

The sand velocity and density data obtained with the monitors, Figures 16(a) and (b) and 17(a) and (b) can be used to estimate the pressure applied to the front of the sample. This is shown in Figures 16(c) and 17(c) for the two standoff distances. The pressure for the 14 cm standoff distance test increased rapidly to a first peak, and then decreased before rising again to a second peak for both cellular structures. This second peak was less apparent for the solid block. The first pressure peak amplitude was 30 MPa for the solid block, 25 MPa for the thick face cellular structure, and 20 MPa for the thin face cellular structure. These peak pressures were nearly identical to the pressures of the initial pressure spike measured using the Hopkinson pressure bars, Table 3, and corresponded to arrival of the fast (spalled) sand at the sample surface. A second, lower pressure of approximately 15 MPa occurred at 0.5 ms after detonation for both cellular structures, and corresponded to the arrival of the more densely packed sand slab at the monitors. Increasing the standoff distance to 40 cm, led to a reduction in sand density (due to axial and lateral stretching of the sand) and a slightly reduced velocity (because of sand-air particle collisions), Figure 17 (a) and (b). This resulted in disappearance of the first pressure spike, Figure 17(c); consistent with the disappearance of the initial spike in pressure observed experimentally, Figure 4, as the standoff distance was increased.

By integrating the hydrodynamic pressure, the impulse-time relation for sand particles could also be calculated, Figures 16(d) and 17(d). At 14 cm, the impulse rose rapidly upon arrival of the sand, and for the solid block reached a maximum of ~13 kPa·s within approximately 2 ms of detonation. The impulse also rose rapidly for both cellular structures, but reached a lower maximum value of approximately 10 kPa·s. This agreed reasonably well with vertical pendulum measurements. Figure 17(d) shows that at a 40 cm standoff distance, the impulse's at the monitor locations were also similar to those measured with the vertical pendulum.

The impulse applied by the particles to the front face of the solid block (located 2.5 cm above the monitors) and both cellular structures (located at 2.7 cm and 1.9 cm above the

monitors for the thin and thick face cellular specimens respectively) could be directly obtained from an output file of the IMPETUS Afea post processor, Figure 18. Good agreement between the vertical pendulum measured and these simulated impulses was seen for all the standoff distances. The impulse-time signals calculated with the contact algorithm exhibit three distinct regions. Region I was associated with impact of the spalled sand at the sand front leading edge. For each standoff distance, the impulse acquired in Region I was almost identical for all three sample types. The slight differences were due to the differing thicknesses of the specimens which slightly changed the standoff distance from that of the solid block. Region II corresponded to impact by the dense sand slug, and was the region most responsible for the impulse differences between the three sample types. Figures 10(d) and 11(d) indicate that Region II corresponds to the period where the separation gap between the steel top plate and the front face of the specimen was rapidly increasing. Recall that the gap for the solid block was smaller than for the cellular structures, and provided less room for sand to escape, and the impulse to remain higher than the crushable cellular structures. Sand loading rapidly decreased in Region III, and corresponded to a regime where the sample to sand box gap was the widest.

6.3 Mechanisms of impulse transfer reduction

(a) Test geometry effects: It has been shown that the combination of the sand box lid deflection, core crushing, and elastic compression (and extension) of the Hopkinson bars all contribute to the gap through which sand flowed away from the sample and escaped the system. To better understand the consequences of this critical aspect of the experiment, the lid was removed from the simulations, keeping the rest of the model unchanged. This allowed the effect of the lid-sample aperture upon the transmitted impulse to be more clearly understood, and reveals the process by which the three samples interact with an unperturbed sand front. Figure 19 shows the transferred impulse (calculated using the sample contact algorithm) to the three sample types at standoff distances of 14 and 40 cm with the sand box lid removed. At a 14 cm standoff, Figure 19(a), the impulse for all three sample types was less than that with the lid in

place, Figure 18(a) because of sand reflection from the inclined periphery of the sand box aperture towards the sample.

These results indicate that the lid aperture substantially affected the impulse transfer, and the mechanisms responsible for this are explored using sand position snap shots shown in Figures 20 and 21. At the 14 cm standoff distance there is no noticeable difference between the simulation with a steel lid and without a steel lid at 0.16 ms after detonation, Figures 10(a) and 20(a). At 0.24 ms after detonation, the spalled sand began to interact with the front face of the sample and the only noticeable difference between the simulation with and without a lid can be seen at the right and left edges of the sand front, Figures 10(b) and 17(b), where the inclined surface defining the aperture is lid has reflected sand into the aperture. At 0.48 ms after detonation the sands peak density with a lid was calculated to be approximately $300\ kg \cdot m^{-3}$ higher than that with no lid present for the three test samples. The monitors calculated no noticeable sand velocity change when the lid was removed. A comparison between Figure 10(c) and Figure 20(c) shows the presence of inclined surface around the aperture of top lid forced some sand that would have otherwise missed the edge of the sample, to coalesce under and then impact the sample. Without a lid, the accumulated (densified) sand below the sample surface assumed a convex shape, and the edges of this dense sand front reflected some of the sand in a manner that allowed a fraction of its vertical impulse to be retained. Continued sand loading at 0.80 ms after detonation showed that without a lid the sand more easily rolled off the samples edge, Figure 20(d), rather than stagnating and eventually escaping as the gap separation increased, Figure 10(d). The formation of this virtual convex sand shape combined with the smaller fraction of the sand slug that impacted the sample resulted in reduced impulse transfer to the sample.

(b) Impact face deformation effects: It is interesting to note that the solid block and the thick face cellular structure acquired a nearly identical impulse once the sand box lid was removed, Figure 19. Figure 20(d) shows that the thick face sheet sample remained nearly planar during sand loading, and the sand flowed off its surface in a similar fashion to the solid block. However, the impulse transmitted to the thin face sheet sample was less than that transmitted to

the solid block, Figure 19. Examination of Figure 20(d) shows that the thin face sheet underwent significant deformation upon spalled sand impact, and its sides were quickly bent upwards to a shape that allowed the subsequent (Region II) sand slab to be only partially arrested before flowing around the specimen. To explore the consequence of this dynamic front face deflection phenomenon, the front face of the thin face cellular structure was again modeled as a 6061 aluminum alloy, but with a greatly increased yield strength (23 GPa) and modulus (7000 GPa) which caused it to remain rigid throughout the simulation.

The red dashed (thin/strong face) line in Figure 19(a) represents the impulse-time response for a cellular sample with a strong thin face sheet that was not allowed to deform. The impulse at 14 cm was increased to that of the solid block, and the thick face cellular structure. It is therefore clear that face sheet deformation was able to promote sand flow around the sample and only partial vertical momentum transfer to the specimen. It is noted that even though the impulse-time response of the three samples reached the same plateau value when the face sheet did not deform, a slight difference in the slope in Region II of the impulse-time response remained, Figure 19(a). The impulse-time response in Region II occurs during core compression, and so the core's contribution to impulse transfer was explored next.

(c) Core strength effects: The cellular structure core has been simulated to this point using an aluminum alloy yield strength of 230 MPa resulting in a core peak crush strength of 21.8 MPa. Since the crush strength of the core scales linearly with that of the alloy's yield strength, the alloy yield strength was progressively decreased in the simulations to investigate how easier core collapse affected the transmitted impulse and applied pressure. The alloy yield strength was decreased to half (115 MPa), a fourth (58 MPa), and an eighth (29 MPa) of its original value, and the core compressive strength calculated using the finite element model developed in the previous study[43]. These core strengths are summarized in Table 4. The sand impact simulations were then repeated without a sandbox lid and a rigid front face was used for all simulations.

Figure 22(a) shows the impulse-time response for cellular structure cores with core compressive strengths between 21.8 and 2.8 MPa. Decreasing the compressive strength of the

cellular structure resulted in a slightly reduced plateaued impulse from 11 kPa·s (for the original core strength of 21.8 MPa) to approximately 10.5 kPa·s for weakest core samples. The approximately 5% decrease in impulse only occurred when the core was sufficiently weak to permit significant core crushing, Figure 22(b-d). The majority of the core crushing occurred during Region I by impact of the spalled sand at the sand front. This allowed the distance between the impact face and the explosive charge original location to rapidly increase (by the product of the original core height and the compressive strain). This increased the standoff distance for later arriving (Region II) sand, and was responsible for the reduction in impulse. To illustrate, if a 7.6 cm thick core weres compressed 50%, the increased standoff distance would be 3.8 cm, and using the slope of the impulse – standoff response for the solid block, Figure 3(a) of *0.2 kPa.s.cm*$^{-1}$, the reduction of impulse if all the sand had impacted at the longer standoff distance would be 0.76 *kPa.s* compared to the 0.5 *kPa.s* change of the simulation.

The collapse sequence in Figure 22(b-e) shows that cellular structures with lower compressive strengths were fully densified 0.8 ms after detonation at a 14 cm standoff distance, Figure 22(e). The maximum velocity attained by the front face during the core crushing Region I response was ~100 ms^{-1}. During the Region I response, the rate of impulse transfer decreased with reduction of core strength, Table 4, because of the decrease in sand impact velocity (and thus stagnation pressure) measured in the front face sheet frame of reference. This result indicates that when a core can be easily compressed by sand impact, the pressure transmitted to the structures distal side can be decreased. We also note no slap enhancement of impulse was observed, even when the core was compressed beyond its densification strain.

7. Concluding Remarks

A vertical pendulum test apparatus has been used to experimentally investigate the impact of explosively accelerated wet sand with back supported Al 6061T6 cellular test structures attached to thin and thick face sheets, and compared to the response of a solid (incompressible) 6061-T6 aluminum block test specimen. The apparatus could be used as a vertical pendulum for determination of the impulse transferred to the specimens when detonation of a 300 g sheet of explosive was used to accelerate a 5.08 cm thick layer of wet silica (sand)

particles towards samples whose flat impact face was inclined at perpendicular to the sand propagation direction. The cellular structures were fabricated from extruded Al6061-T6 square tubes that were arranged in a rectilinear pattern and had a relative density of $\bar{\rho} = 20.1\%$. Instrumented Hopkinson bars attached to the rear face of the samples also enabled the pressure exerted on the sample to be measured. Integration of these pressure waveforms over time enabled an independent estimate of the transferred impulse for 558 μs after the start of sand impact to be measured. By varying the distance between the surface of the explosive layer and the samples front face from 14 to 40 cm, the transferred impulse and pressure were found to decrease with distance for all tested samples. A particle base simulation implemented in the IMPETUS Afea Solver was used to model the experiments and excellent agreement was observed between the experimental and simulation results. This validated code was then used to investigate the mechanisms of the sand-structure interaction with cellular structures. It has been found that:

1. When cellular structures were placed just above the aperture in the lid of the sand containment box, the transmitted impulse to cellular structures was reduced by approximately 10-15% compared to that transmitted to a solid block at the closest standoff distances. This change decreased to zero as the standoff distance increased and was correlated with reduced sample compression. The pressure transmitted to the distal end of the specimen was also shown to be reduced by cellular structure that underwent significant plastic compression.
2. Particle based simulations accurately predict the impulse transferred during the vertical mode tests and the pressure waveforms recorded with the instrumented Hopkinson pressure bars. In addition, the cores deformation modes were accurately predicted along with the percentage of core strain and the change in impulse.
3. The simulations provided a means to investigate the soil structure interaction and revealed that the gap between the samples front face and the sand box top was largely responsible for the reduction in impulse. The separation gap acted as a valve to allow sand to escape from the system and release sand pressure. Compressible structures with easily deformed faces were shown to enable a more significant opening and greater impulse reduction.

4. By making the thin front face sheet rigid and removing the sand box lid in the simulations, it has been shown that strong core cellular structures transferred the same impulse as a solid block. Identical cores with soft impact faces transferred less impulse than the solid block because they dynamically deformed to a convex shape, which reduced the vertical component of sand momentum transferred to the specimen.
5. As the core crush strength was reduced in simulations, a small (~5%) sand-structure interaction was observed with the sand box lid removed and the thin front face forced to be rigid. This effect resulted from a dynamic increase in standoff distance due to core compression. A weak core was also shown to decrease the impulse transfer rate (and therefore acceleration) applied to the distal end of the specimen.
6. The study has shown that in contrast to underwater shock loading at zero obliquity,[22, 23] the impact of explosively accelerated sand against a soft (compressible) structure that remains planar during impact, results in no significant reduction of the transferred momentum. More substantial reductions in the rate of momentum transfer (and thus pressure applied to the protected structure) can be accomplished by thick core cellular structures with core strengths that are 0.1-0.5 that of the hydrodynamic pressure applied by the sand.

Acknowledgements

The authors are grateful to Keith Williams of NEWTEC Services Group, Inc. for his excellent technical help and guidance, and to Dr. Kumar Dharmasena, Tommy Eanes, and Adam Malcom for experimental assistance. We are grateful to both the U.S. Office of Naval Research (ONR grant number N00014-07-1-0764) managed by Dr. David Shifler and DARPA (DARPA grant number W91CRB-11-1-0005), managed by Dr. Judah Goldwasser for co-supporting this study.

References

[1] Gibson, L.J., and M.F. Ashby. *Cellular Solids: Structure and Properties*. 2nd ed. Cambridge: Cambridge University Press, 1997.

[2] Smith, P.D., and J.G. Hetherington. *Blast and Ballistic Loading of Structures*. Oxford: Butterworth-Heinemann, 1994.

[3] Mills, N. *Polymer Foams Handbook: Engineering and Biomechanics Applications and Design Guide*. 1st ed. Oxford: Butterworth-Heinemann, 2007.

[4] Ashby, M.F., A.G. Evans, N. A. Fleck, L.J. Gibson, J.W. Hutchinson, and H.N.G. Wadley. *Metal Foams: A Design Guide*. Butterworth-Heinemann, 2000.

[5] Wadley, H.N.G., K.P. Dharmasena, M.Y. He, R.M. McMeeking, A.G. Evans, T. Bui-Thanh, and R. Radovitzky. "An Active Concept for Limiting Injuries Caused by Air Blasts." *International Journal of Impact Engineering* 37, no. 3 (March 2010): 317–23. doi:10.1016/j.ijimpeng.2009.06.006.

[6] Queheillalt, Douglas T., and Haydn N. G. Wadley. "Hollow Pyramidal Lattice Truss Structures." *International Journal of Materials Research* 102, no. 4 (April 2011): 389–400. doi:10.3139/146.110489.

[7] Dunand, D. C. "Processing of Titanium Foams." *Advanced Engineering Materials* 6, no. 6 (June 2004): 369–76. doi:10.1002/adem.200405576.

[8] Wei, Z., K.P. Dharmasena, H.N.G. Wadley, and A.G. Evans. "Analysis and Interpretation of a Test for Characterizing the Response of Sandwich Panels to Water Blast." *International Journal of Impact Engineering* 34, no. 10 (October 2007): 1602–1618. doi:10.1016/j.ijimpeng.2006.09.091.

[9] Deshpande, V, and N Fleck. "One-dimensional Response of Sandwich Plates to Underwater Shock Loading." *Journal of the Mechanics and Physics of Solids* 53, no. 11 (November 2005): 2347–2383. doi:10.1016/j.jmps.2005.06.006.

[10] Liang, Y., A.V. Spuskanyuk, S.E. Flores, D.R. Hayhurst, J.W. Hutchinson, R.M. McMeeking, and A.G. Evans. "The Response of Metallic Sandwich Panels to Water Blast." *Journal of Applied Mechanics* 74, no. 1 (2007): 81–99.

[11] Tilbrook, M.T., V.S. Deshpande, and N.A. Fleck. "Underwater Blast Loading of Sandwich Beams: Regimes of Behaviour." *International Journal of Solids and Structures* 46, no. 17 (August 2009): 3209–21. doi:10.1016/j.ijsolstr.2009.04.012.

[12] Liang, Yueming, Alexander V. Spuskanyuk, Shane E. Flores, David R. Hayhurst, John W. Hutchinson, Robert M. McMeeking, and Anthony G. Evans. "The Response of Metallic Sandwich Panels to Water Blast." *Journal of Applied Mechanics* 74, no. 1 (2007): 81. doi:10.1115/1.2178837.

[13] Qiu, X., V. S. Deshpande, and N. A. Fleck. "Dynamic Response of a Clamped Circular Sandwich Plate Subject to Shock Loading." *Journal of Applied Mechanics* 71, no. 5 (2004): 637. doi:10.1115/1.1778416.

[14] Deshpande, V.S., A. Heaver, and N.A. Fleck. "An Underwater Shock Simulator." *Proceedings of the Royal Society A: Mathematical, Physical and Engineering Sciences* 462, no. 2067 (March 8, 2006): 1021–41. doi:10.1098/rspa.2005.1604.

[15] Espinosa, H. D., S. Lee, and N. Moldovan. "A Novel Fluid Structure Interaction Experiment to Investigate Deformation of Structural Elements Subjected to Impulsive Loading." *Experimental Mechanics* 46, no. 6 (December 2006): 805–24. doi:10.1007/s11340-006-0296-7.

[16] Taylor, G.I. *The Pressure and Impulse of Submarine Explosion Waves on Plates*. Vol. III. Cambridge University Press, 1963.

[17] Fleck, N. A., and V. S. Deshpande. "The Resistance of Clamped Sandwich Beams to Shock Loading." *Journal of Applied Mechanics* 71, no. 3 (2004): 386. doi:10.1115/1.1629109.

[18] Xue, Zhenyu, and John W. Hutchinson. "A Comparative Study of Impulse-resistant Metal Sandwich Plates." *Int. J. Impact Engng* 30, no. 10 (November 2004): 1283–1305. doi:10.1016/j.ijimpeng.2003.08.007.

[19] Chen, Yong, Z.P. Tong, H.X. Hua, Y. Wang, and H.Y. Gou. "Experimental Investigation on the Dynamic Response of Scaled Ship Model with Rubber Sandwich Coatings Subjected to Underwater Explosion." *International Journal of Impact Engineering* 36, no. 2 (February 2009): 318–328. doi:10.1016/j.ijimpeng.2007.12.015.

[20] Chen, Yong, ZhiYi Zhang, Yu Wang, and Hongxing Hua. "Crush Dynamics of Square Honeycomb Thin Rubber Wall." *Thin-Walled Structures* 47, no. 12 (December 2009): 1447–1456. doi:10.1016/j.tws.2009.07.007.

[21] Schiffer, A., and V. L. Tagarielli. "The Response of Rigid Plates to Blast in Deep Water: Fluid-structure Interaction Experiments." *Proceedings of the Royal Society A: Mathematical, Physical and Engineering Sciences* 468, no. 2145 (May 9, 2012): 2807–2828. doi:10.1098/rspa.2012.0076.

[22] Dharmasena, Kumar, Doug Queheillalt, Haydn Wadley, Yungchia Chen, Philip Dudt, David Knight, Zhensong Wei, and Anthony Evans. "Dynamic Response of a Multilayer Prismatic Structure to Impulsive Loads Incident from Water." *International Journal of Impact Engineering* 36, no. 4 (April 2009): 632–643. doi:10.1016/j.ijimpeng.2008.06.002.

[23] Dharmasena, K.P., D.T. Queheillalt, H.N.G. Wadley, P. Dudt, Y. Chen, D. Knight, A.G. Evans, and V.S. Deshpande. "Dynamic Compression of Metallic Sandwich Structures During Planar Impulsive Loading in Water." *European Journal of Mechanics - A/Solids* 29, no. 1 (January 2010): 56–67. doi:10.1016/j.euromechsol.2009.05.003.

[24] Mori, L.F., S. Lee, Z.Y. Xue, A. Vaziri, D.T. Queheillalt, K.P. Dharmasena, H.N.G. Wadley, J.W. Hutchinson, and H.D. Espinosa. "Deformation and Fracture Modes of Sandwich Structures Subjected to Underwater Impulsive Loads." *Journal of Mechanics of Materials and Structures* 2, no. 10 (2007): 1981–2006.

[25] Mori, L. F., D. T. Queheillalt, H. N. G. Wadley, and H. D. Espinosa. "Deformation and Failure Modes of I-Core Sandwich Structures Subjected to Underwater Impulsive Loads." *Experimental Mechanics* 49, no. 2 (September 4, 2008): 257–275. doi:10.1007/s11340-008-9166-9.

[26] Wei, Z., V.S. Deshpande, A.G. Evans, K.P. Dharmasena, D.T. Queheillalt, H.N.G. Wadley, Y.V. Murty, et al. "The Resistance of Metallic Plates to Localized Impulse." *Journal of the Mechanics and Physics of Solids* 56, no. 5 (May 2008): 2074–2091. doi:10.1016/j.jmps.2007.10.010.

[27] Wadley, Haydn, Kumar Dharmasena, Yungchia Chen, Philip Dudt, David Knight, Robert Charette, and Kenneth Kiddy. "Compressive Response of Multilayered Pyramidal Lattices During Underwater Shock Loading." *International Journal of Impact Engineering* 35, no. 9 (September 2008): 1102–1114. doi:10.1016/j.ijimpeng.2007.06.009.

[28] McShane, G.J., D.D. Radford, V.S. Deshpande, and N.A. Fleck. "The Response of Clamped Sandwich Plates with Lattice Cores Subjected to Shock Loading." *European Journal of Mechanics - A/Solids* 25, no. 2 (March 2006): 215–229. doi:10.1016/j.euromechsol.2005.08.001.

[29] Radford, D.D., G.J. McShane, V.S. Deshpande, and N.A. Fleck. "The Response of Clamped Sandwich Plates with Metallic Foam Cores to Simulated Blast Loading." *International Journal of Solids and Structures* 43, no. 7–8 (April 2006): 2243–2259. doi:10.1016/j.ijsolstr.2005.07.006.

[30] Kambouchev, Nayden, Raul Radovitzky, and Ludovic Noels. "Fluid–Structure Interaction Effects in the Dynamic Response of Free-Standing Plates to Uniform Shock Loading." *Journal of Applied Mechanics* 74, no. 5 (2007): 1042. doi:10.1115/1.2712230.

[31] Hutchinson, John W., and Zhenyu Xue. "Metal Sandwich Plates Optimized for Pressure Impulses." *International Journal of Mechanical Sciences* 47, no. 4–5 (April 2005): 545–69. doi:10.1016/j.ijmecsci.2004.10.012.

[32] Neuberger, A., S. Peles, and D. Rittel. "Scaling the Response of Circular Plates Subjected to Large and Close-range Spherical Explosions. Part II: Buried Charges." *International Journal of Impact Engineering* 34, no. 5 (May 2007): 874–882. doi:10.1016/j.ijimpeng.2006.04.002.

[33] Luccioni, Bibiana, Daniel Ambrosini, Steeve Chung Kim Yuen, and Gerald Nurick. "Effects of Large and Spread Explosives Loads." *International Journal of Protective Structures* 1, no. 3 (September 1, 2010): 319–344. doi:10.1260/2041-4196.1.3.319.

[34] Dharmasena, Kumar P., Haydn N.G. Wadley, Tao Liu, and Vikram S. Deshpande. "The Dynamic Response of Edge Clamped Plates Loaded by Spherically Expanding Sand Shells." *International Journal of Impact Engineering* 62 (December 2013): 182–195. doi:10.1016/j.ijimpeng.2013.06.012.

[35] Liu, T., N.A. Fleck, H.N.G. Wadley, and V.S. Deshpande. "The Impact of Sand Slugs Against Beams and Plates: Coupled Discrete Particle/finite Element Simulations." *Journal of the Mechanics and Physics of Solids* 61, no. 8 (August 2013): 1798–1821. doi:10.1016/j.jmps.2013.03.008.

[36] McShane, G.J., V.S. Deshpande, and N.A. Fleck. "A Laboratory-scale Buried Charge Simulator." *International Journal of Impact Engineering* 62 (December 2013): 210–218. doi:10.1016/j.ijimpeng.2013.06.007.

[37] Pickering, E.G., S. Chung Kim Yuen, G.N. Nurick, and P. Haw. "The Response of Quadrangular Plates to Buried Charges." *International Journal of Impact Engineering* 49 (November 2012): 103–114. doi:10.1016/j.ijimpeng.2012.05.007.

[38] Børvik, T., L. Olovsson, A.G. Hanssen, K.P. Dharmasena, H. Hansson, and H.N.G. Wadley. "A Discrete Particle Approach to Simulate the Combined Effect of Blast and Sand Impact Loading of Steel Plates." *Journal of the Mechanics and Physics of Solids* 59, no. 5 (May 2011): 940–958. doi:10.1016/j.jmps.2011.03.004.

[39] Wadley, H.N.G., T. Børvik, L. Olovsson, J.J. Wetzel, K.P. Dharmasena, O.S. Hopperstad, V.S. Deshpande, and J.W. Hutchinson. "Deformation and Fracture of Impulsively Loaded Sandwich Panels." *Journal of the Mechanics and Physics of Solids* 61, no. 2 (February 2013): 674–699. doi:10.1016/j.jmps.2012.07.007.

[40] Park, S., T. Uth, N.A. Fleck, H.N.G. Wadley, and V.S. Deshpande. "Sand Column Impact onto a Kolsky Pressure Bar." *International Journal of Impact Engineering* 62 (December 2013): 229–42. doi:10.1016/j.ijimpeng.2013.07.003.

[41] Holloman, R.L., V. S. Deshpande, and H.N.G. Wadley. "Impulse Transfer during Sand Impact with a Solid Block," *International Journal of Impact Engineering* 76 (2015): 98-117: doi.org/10.1016/j.ijimpeng.2014.09.010.

[42] Liu, T., H.N.G. Wadley, and V.S. Deshpande. "Dynamic Compression of Foam Supported Plates Impacted by High Velocity Soil." *International Journal of Impact Engineering* 63 (January 2014): 88–105. doi:10.1016/j.ijimpeng.2013.08.004.

[43] Holloman, Ryan L., Vikram Deshpande, Arve G. Hanssen, Katherine M. Fleming, John R. Scully, and Haydn N. G. Wadley. "Tubular Aluminum Cellular Structures: Fabrication and Mechanical Response." *Journal of Mechanics of Materials and Structures* 8, no. 1 (2013): 65–94. doi:10.2140/jomms.2013.8.65.

[44] Holloman, Ryan L., Karthikeyan Kandan, Vikram Deshpande, and Haydn N. G. Wadley. "Dynamic Compression of Square Tube Cellular Structures." *Journal of Mechanics of Materials and Structures* 9, no. 2 (2014): 149-182. doi:10.2140/jomms.2014.9.149.

[45] "Welcome to IMPETUS AFEA." Accessed February 11, 2014. http://www.impetus-afea.com/.

[46] Olovsson, L., Hanssen, A.G.,Børvik,T., Langseth,M., "A particle-based approach to close-range blast loads", European Journal of Mechanics-A/Solids, 29, (2010) 1–6.

[47] Zok, F. W., H. Rathbun, M. He, E. Ferri, C. Mercer, R. M. McMeeking, and A. G. Evans. "Structural Performance of Metallic Sandwich Panels with Square Honeycomb Cores." *Philosophical Magazine* 85, no. 26–27 (September 11, 2005): 3207–3234. doi:10.1080/14786430500073945.

[48] Radford, D. D., G. J. McShane, V. S. Deshpande, and N. A. Fleck. "Dynamic Compressive Response of Stainless-Steel Square Honeycombs." *Journal of Applied Mechanics* 74, no. 4 (2007): 658. doi:10.1115/1.2424717.

[49] Fyllingen, ø., O.S. Hopperstad, A.G. Hanssen, and M. Langseth. "Modelling of Tubes Subjected to Axial Crushing." *Thin-Walled Structures* 48, no. 2 (February 2010): 134–142. doi:10.1016/j.tws.2009.08.007.

[50] Cockcroft, M.G., and D.J Latham. "Ductility and the Workability of Metals." *J. Inst. Metals* 96, no. 1 (1968): 33–39.

Figures and Tables

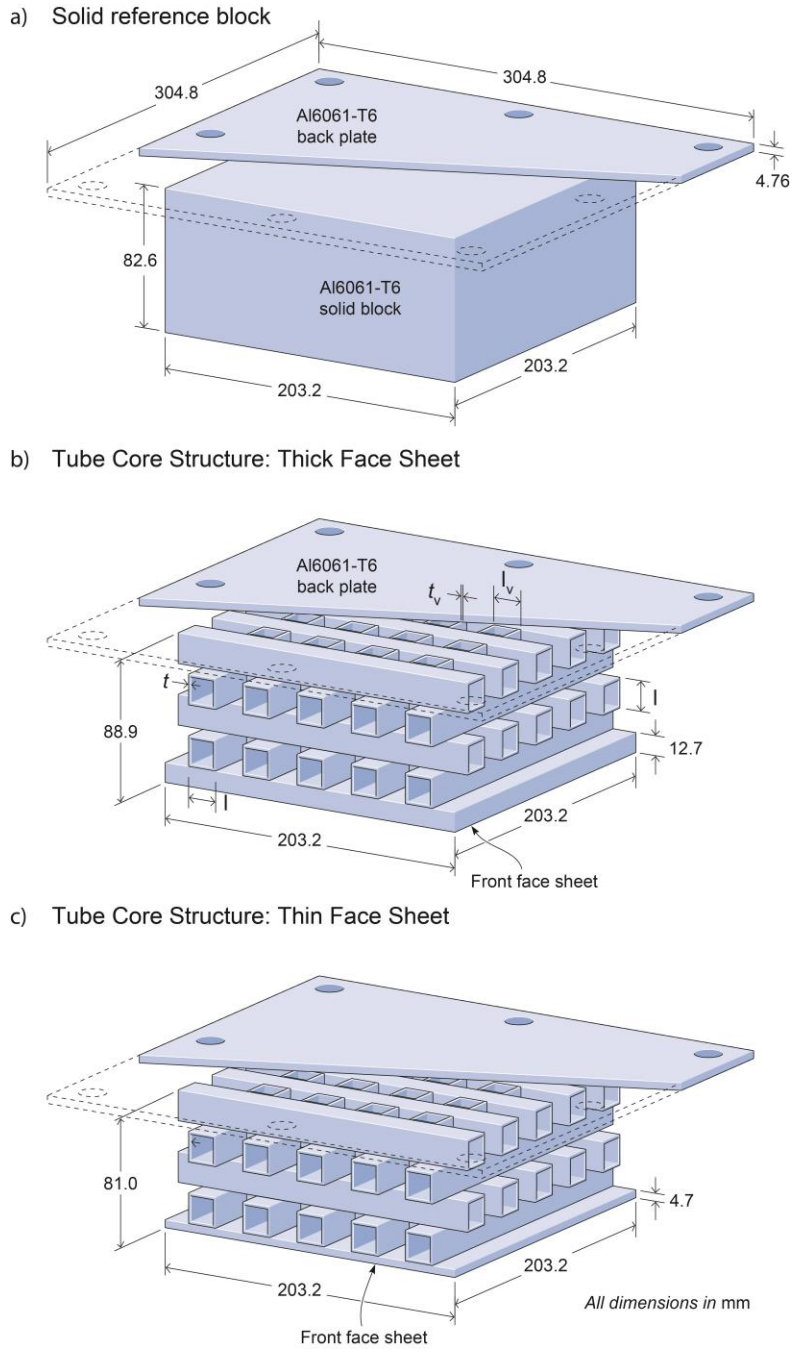

Figure 1. The back-supported test structures used for the sand impact loading experiments. (a) Solid Al6061-T6 reference block welded to 4.76 mm thick plate. The hole pattern on the back face sheet provided a means to bolt the specimen to the vertical impulse test apparatus. (b) The Al6061-T6 3D tube cellular structure with 12.7 mm thick front face and (c) the same cellular structure with a 4.7 mm thin front face.

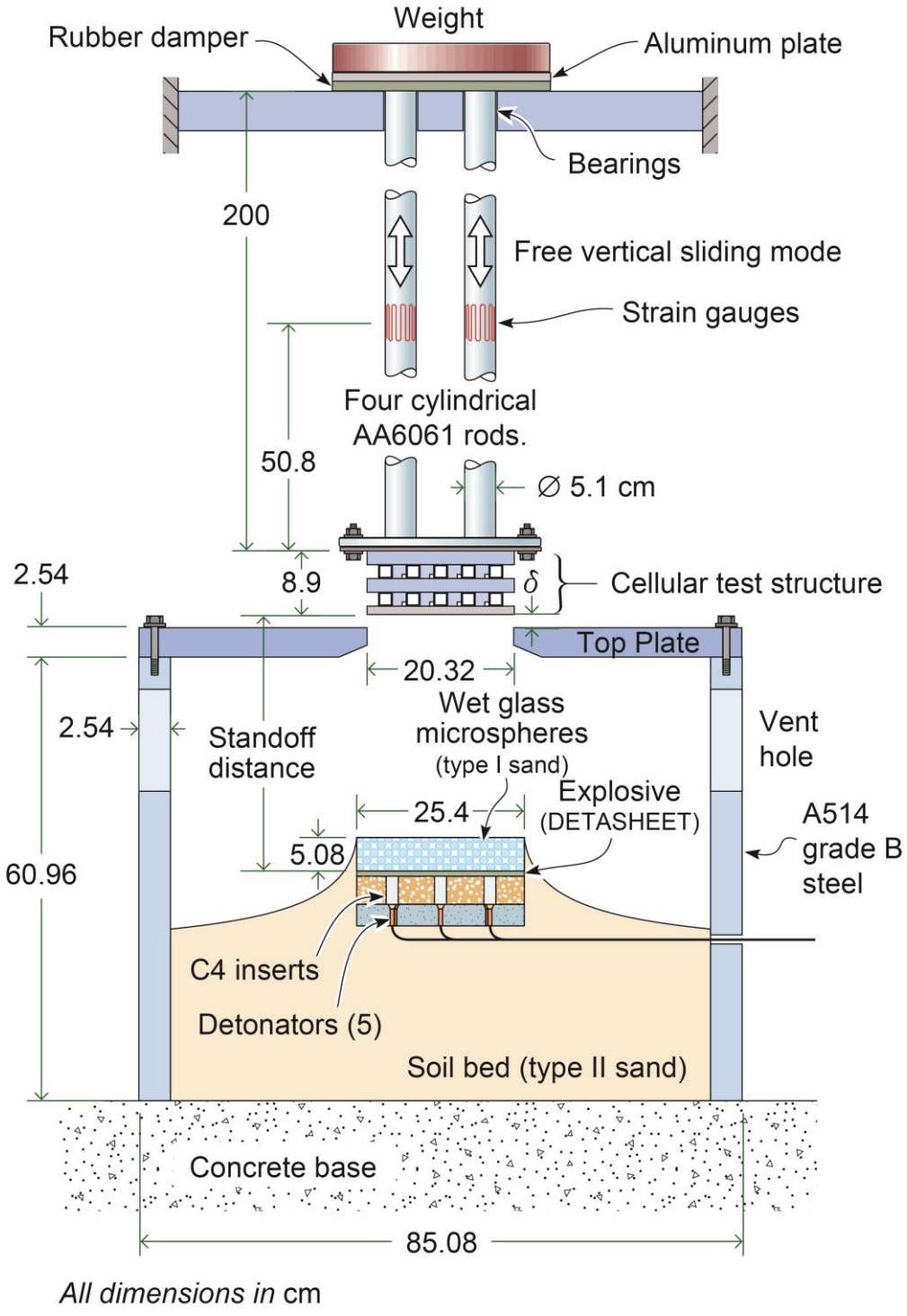

Figure 2. The vertical impulse test apparatus used to measure impulse and pressure transmission by the three test samples during synthetic sand impact. The standoff distance was varied by raising or lowering the location of the explosive sheet within the soil bed. The initial gap δ between sample surface and the sandbox top plate was 8.1 mm for the solid block, 9.7 mm for the thin face sheet cellular structure, and 1.8 mm for the thick face sheet samples.

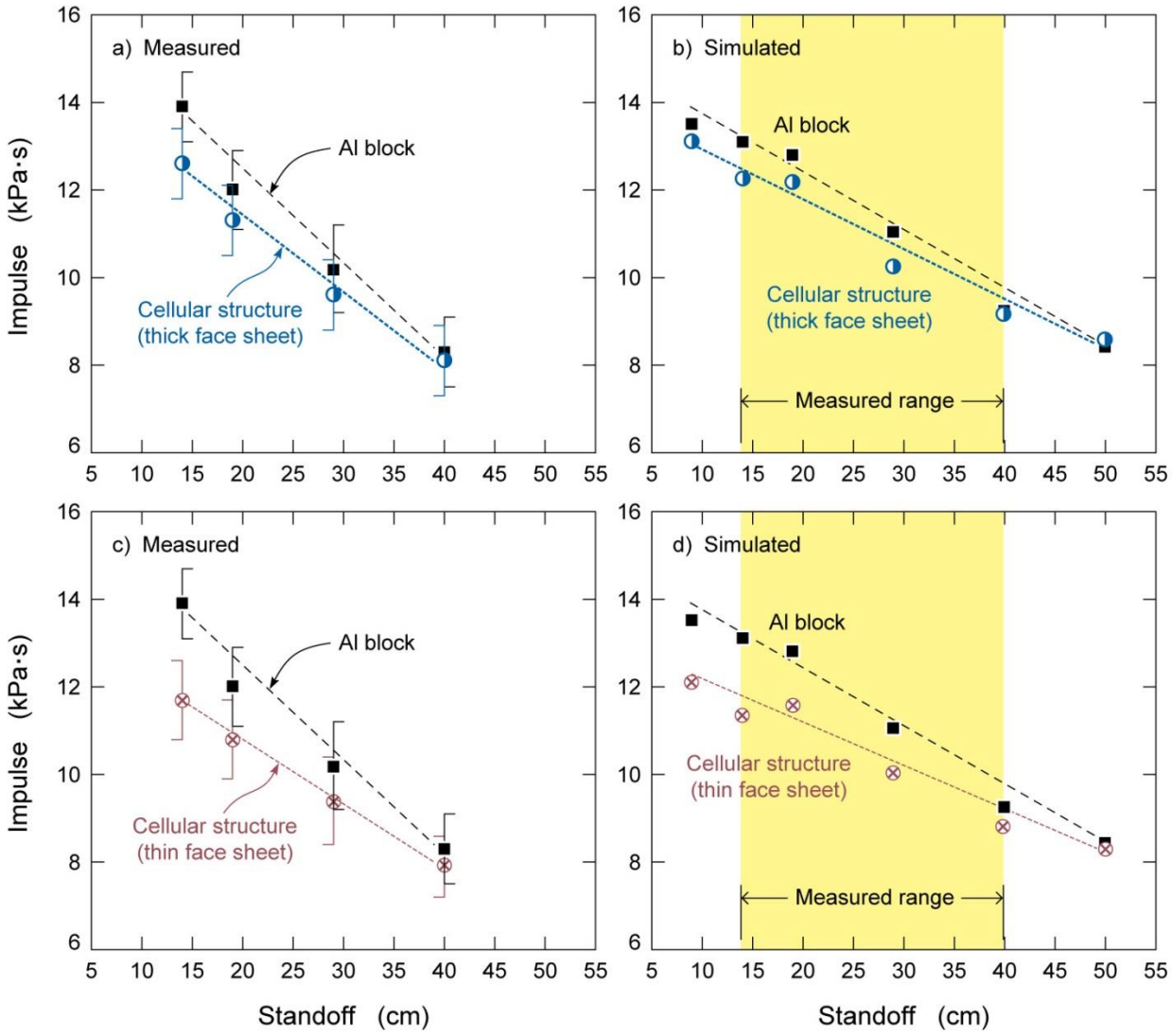

Figure 3. (a) Comparison between experimentally measured impulses transmitted by a solid aluminum block and the cellular structure with a thick front face versus standoff distance. (b) Simulated results for the same experiments. (c) Comparison between experimentally measured impulses transmitted to a solid aluminum block and cellular sample with a thin front face versus standoff distance. (b) Simulated results for the same experiments together with extensions to establish trends.

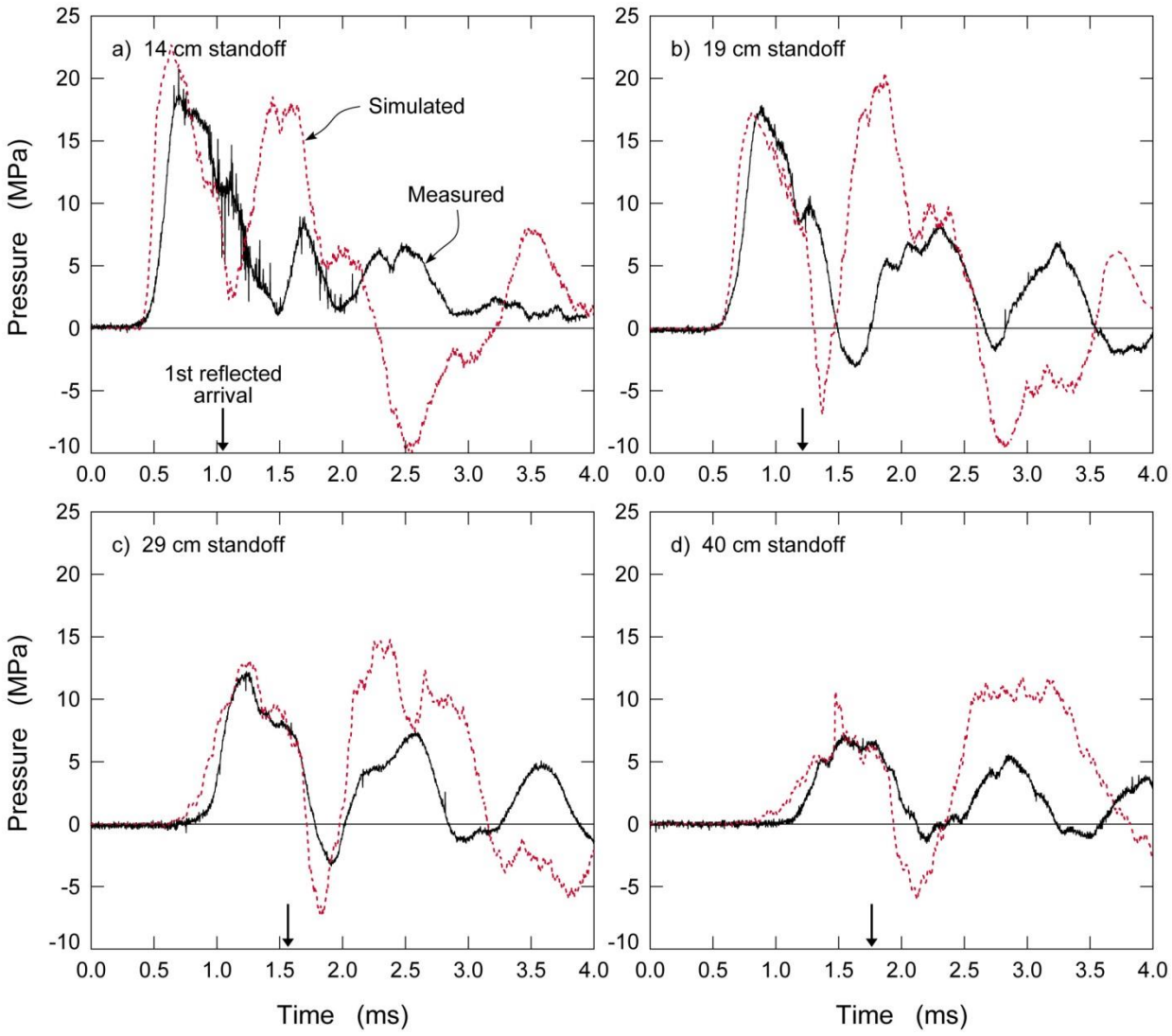

Figure 4. Measured (solid line) and simlulated pressure-time waveforms for the thin face sheet cellular structure at standoff distances of a) 14 cm, b) 19 cm, c) 24cm, and d) 40 cm.

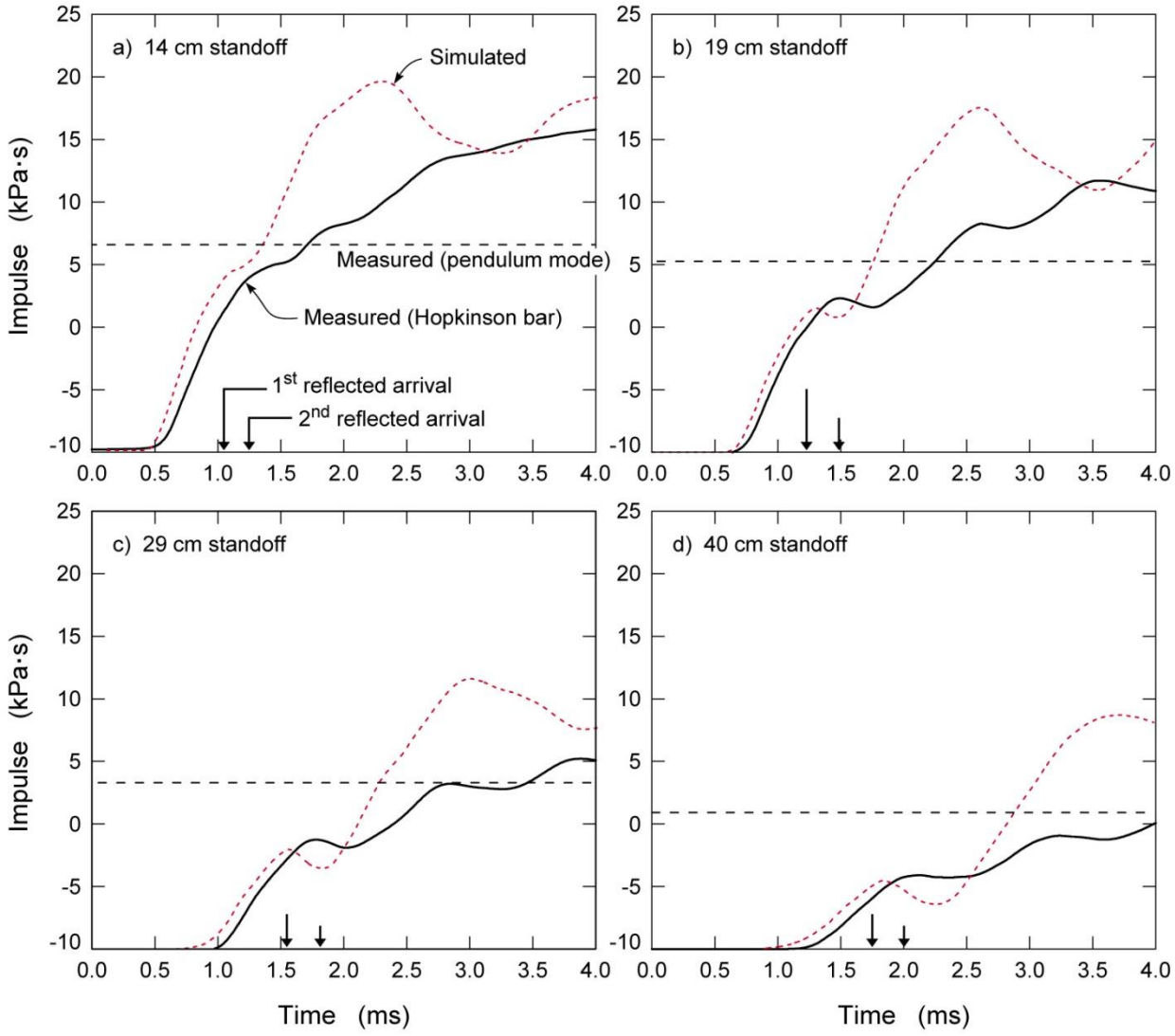

Figure 5. Measured and simulated transmitted impulse-time waveforms obtained by integration of the pressure-time waveforms for the thin face sheet cellular structure for standoff distances of a) 14 cm, b) 19 cm, c) 24cm, and d) 40 cm.

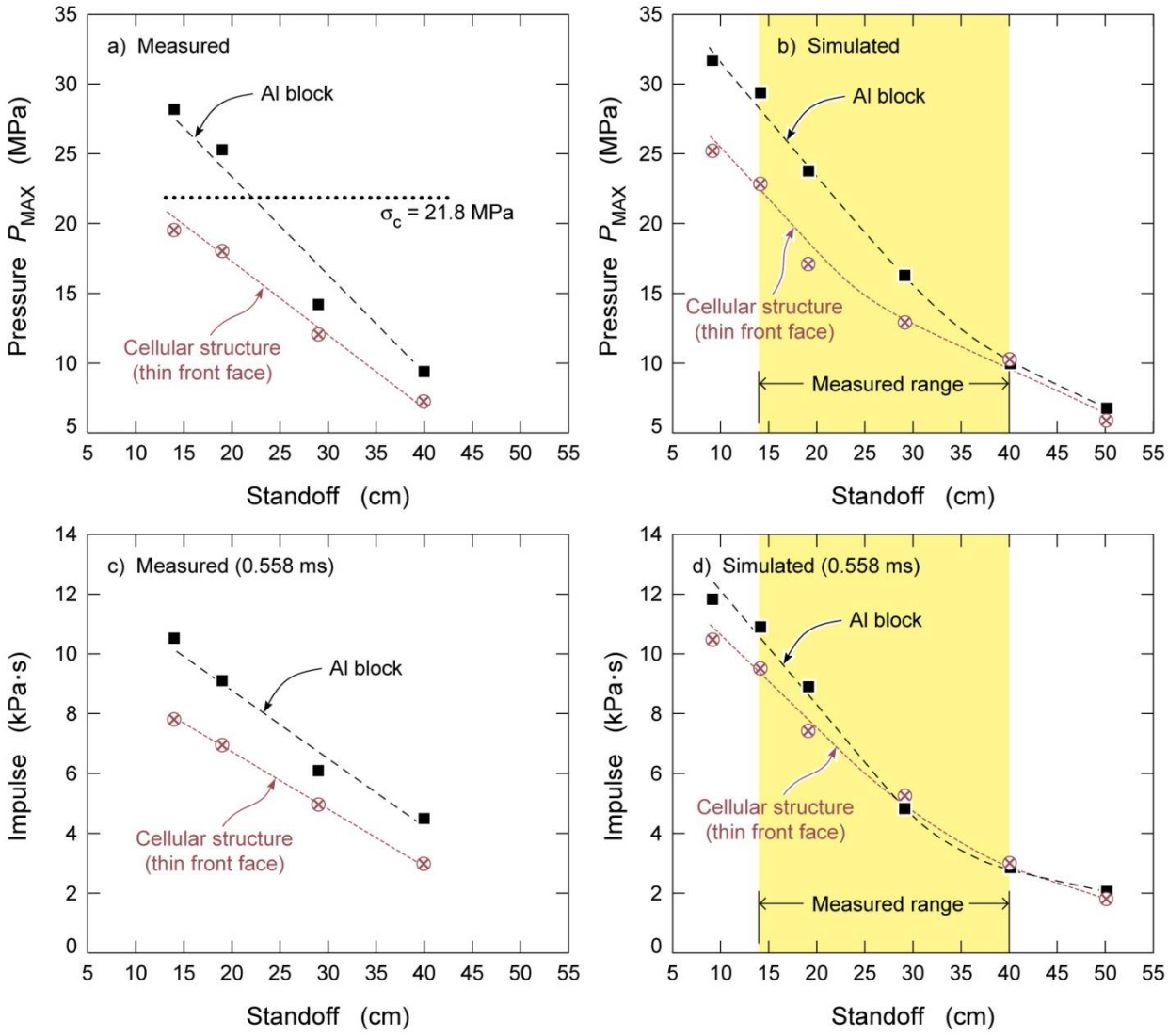

Figure 6. The dependence of maximum pressure transmitted to the distal side of the solid aluminum block and thin faced cellular structure versus standoff distance; a) measured and b) simulated. The standoff distance dependence of impulse transmitted to the solid aluminum block and a thin faced cellular structure during 558 μs of sand loading; c) determined by integration of measured pressure - time response and d) determined by integration of simulated pressure – time responses.

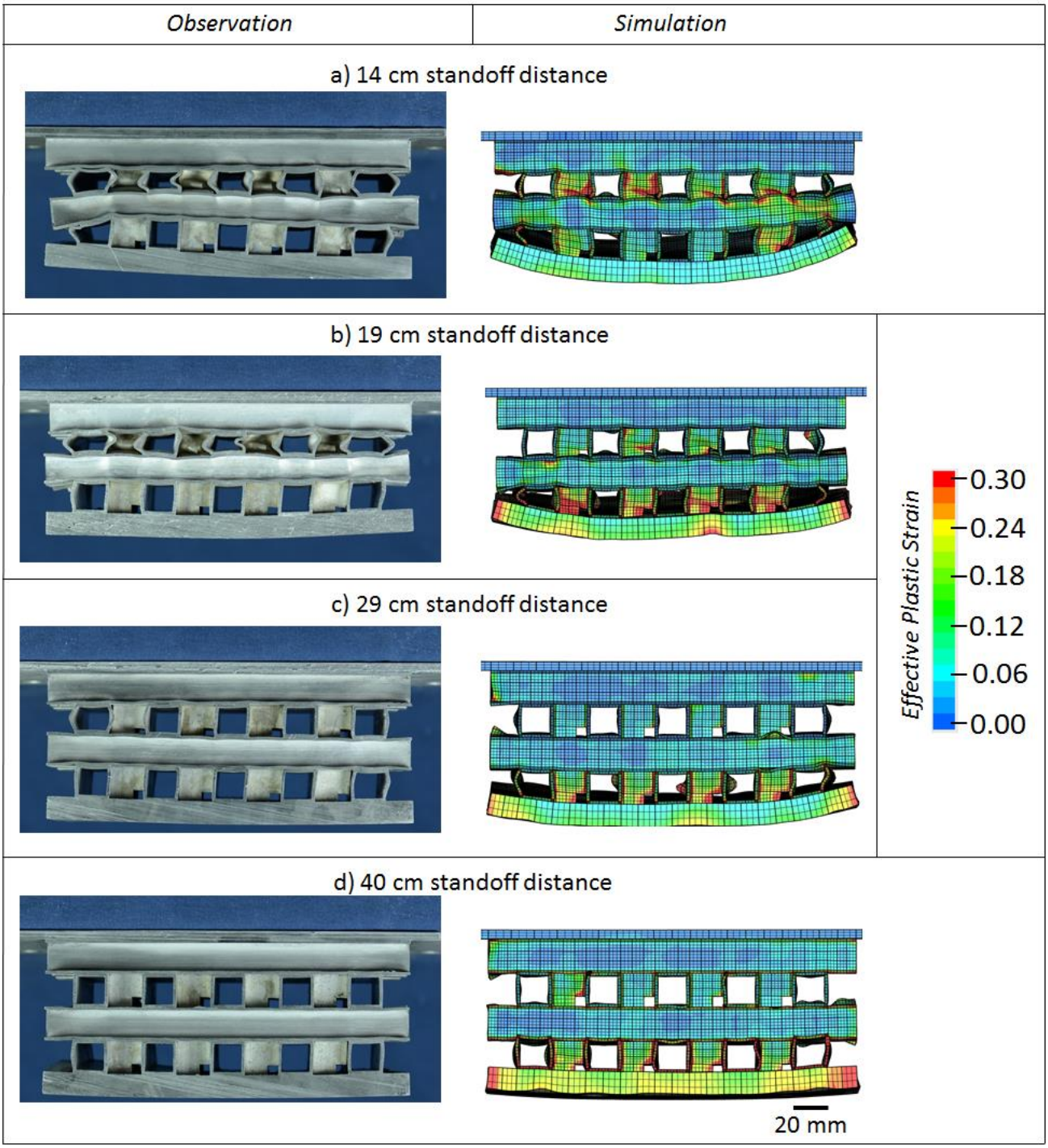

Figure 7. Comparison of measured and simulated deformations of the thick face cellular structure following impulsive sand loading (from below) at various standoff distances.

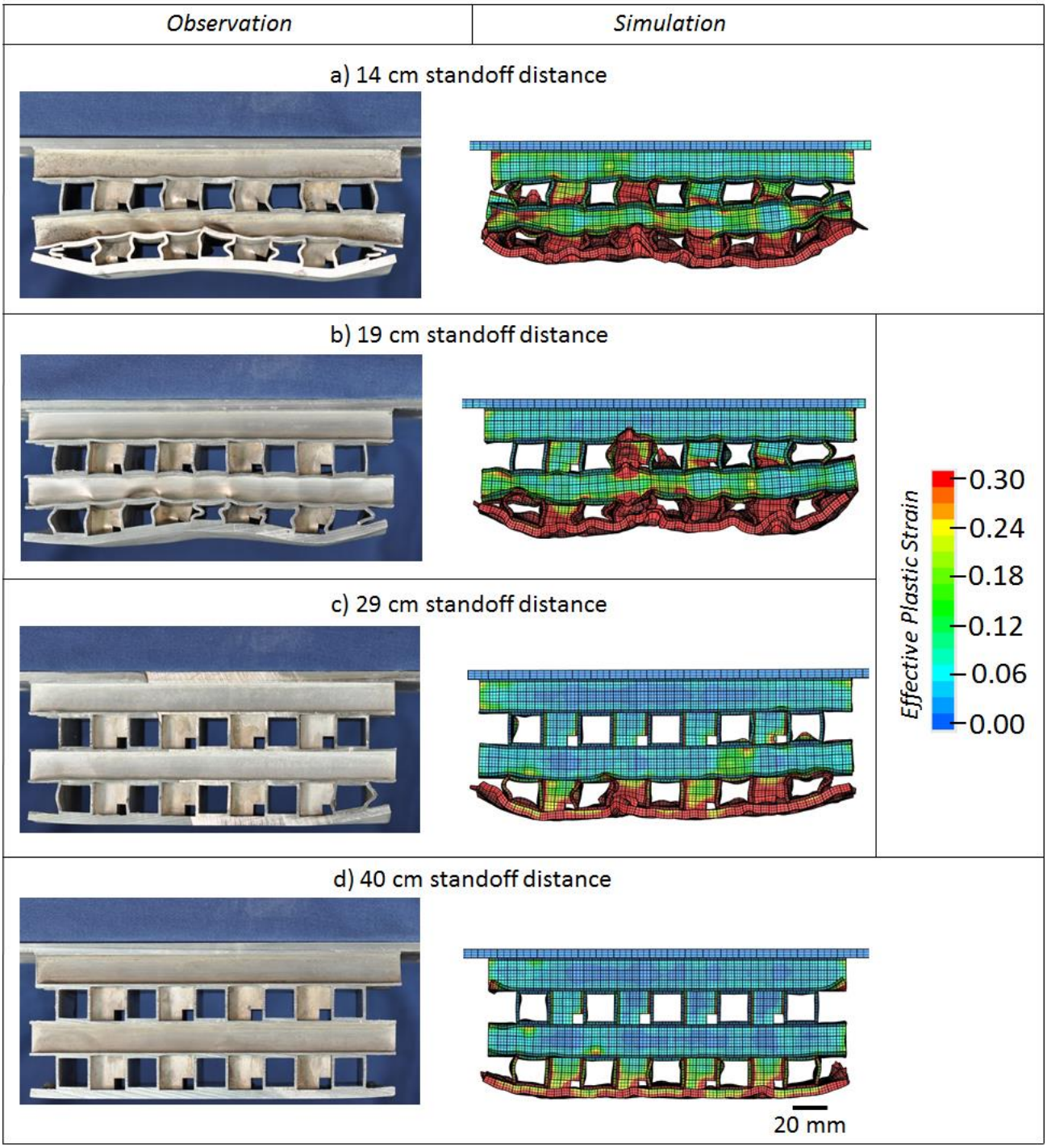

Figure 8. Comparison of measured and simulated cross-sectional images of the thin face cellular test structure after sand impact at stand off distances of a) 14cm, b) 19cm, c) 29cm, and d) 40cm.

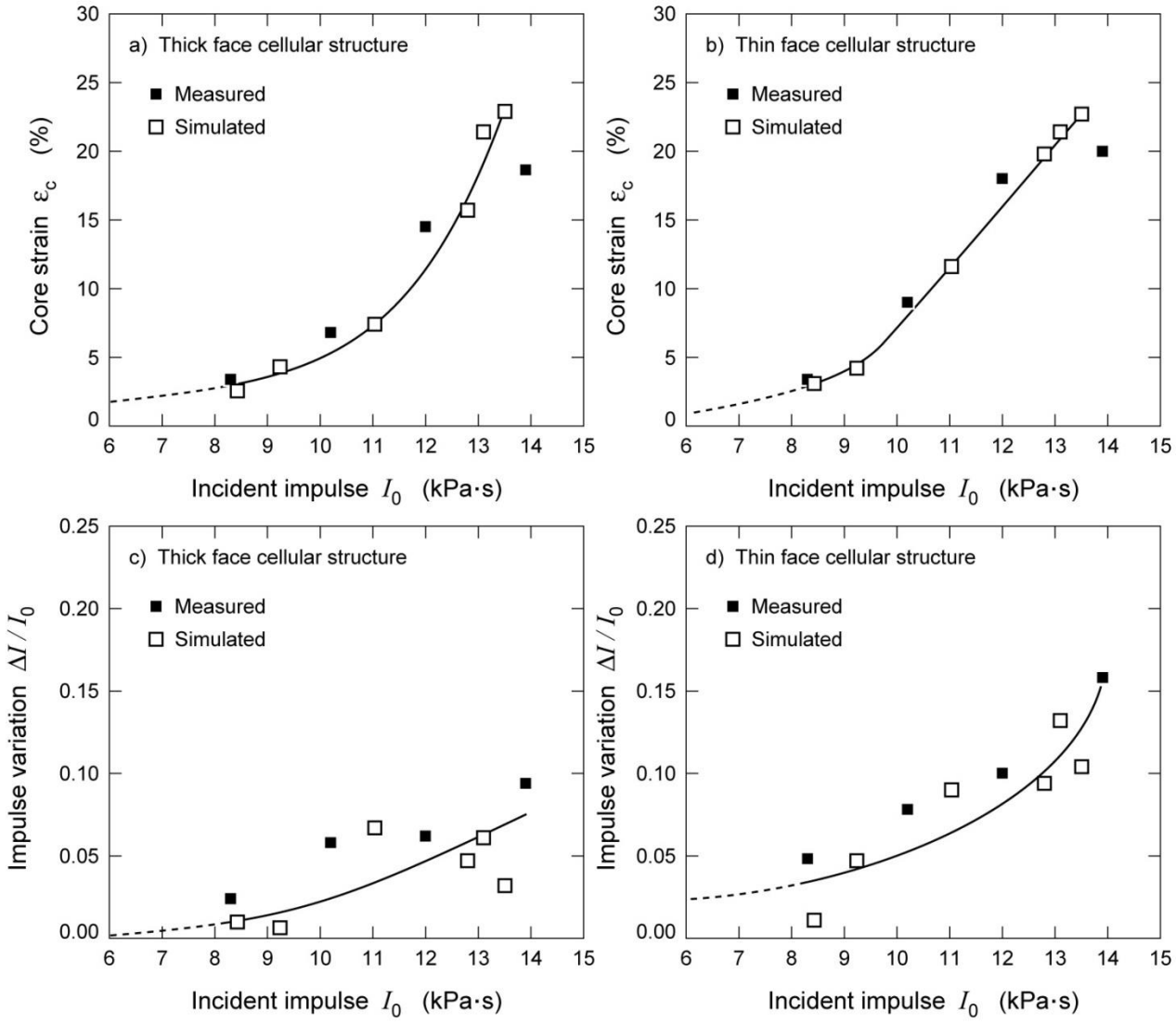

Figure 9. a) Core compressive strain versus incident impulse for the thick face cellular, and b) thin face cellular structures. c) The difference in transmitted impulse between a solid aluminum block and the thick face cellular structure versus the incident impulse. d) Shows the difference in transmitted impulse between a solid block and the thin face cellular structure.

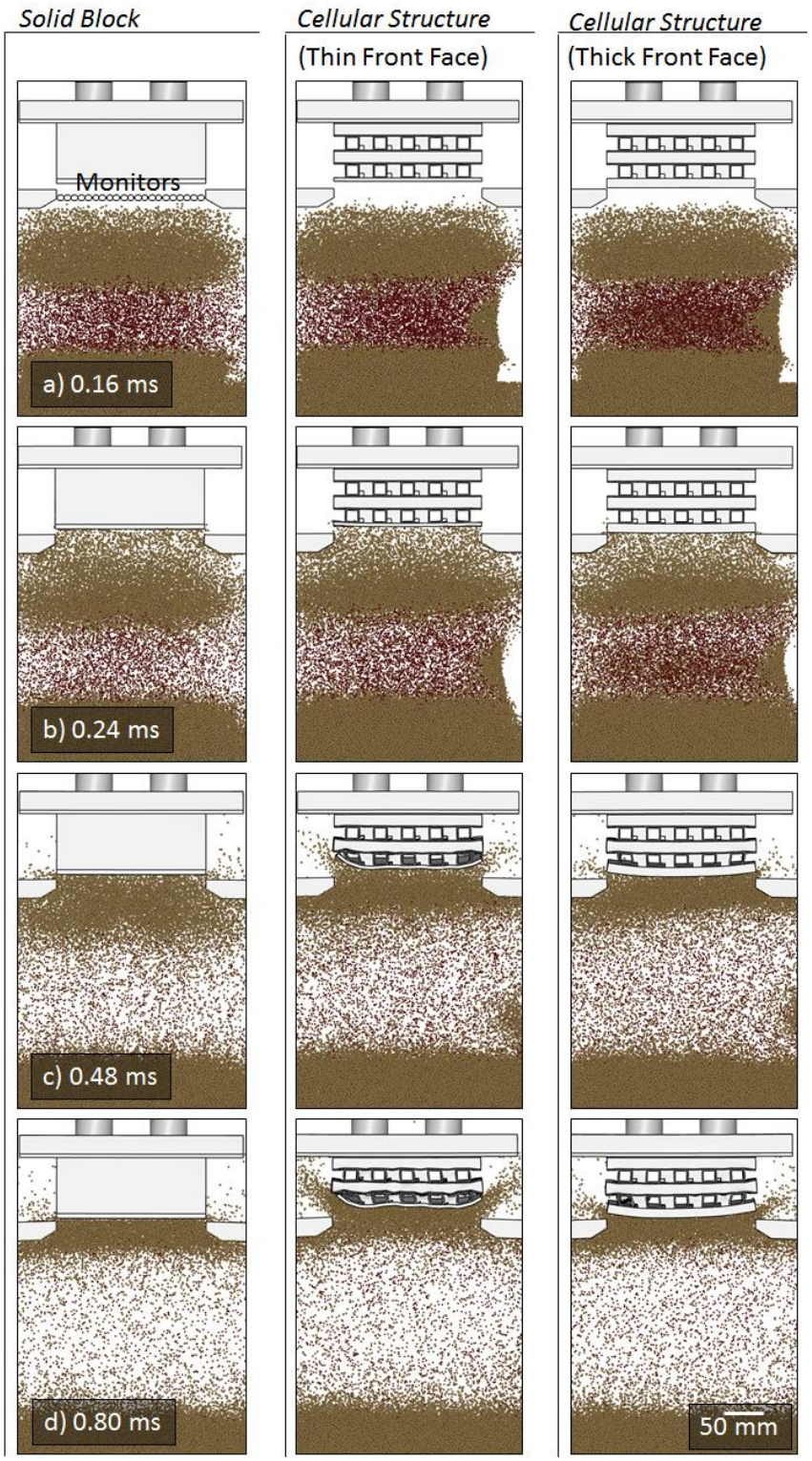

Figure 10. A simulated sand particle propagation sequence for a solid block, a thin faced sandwich structure and a thick faced sandwich structure at a nominal standoff distance of 14 cm.

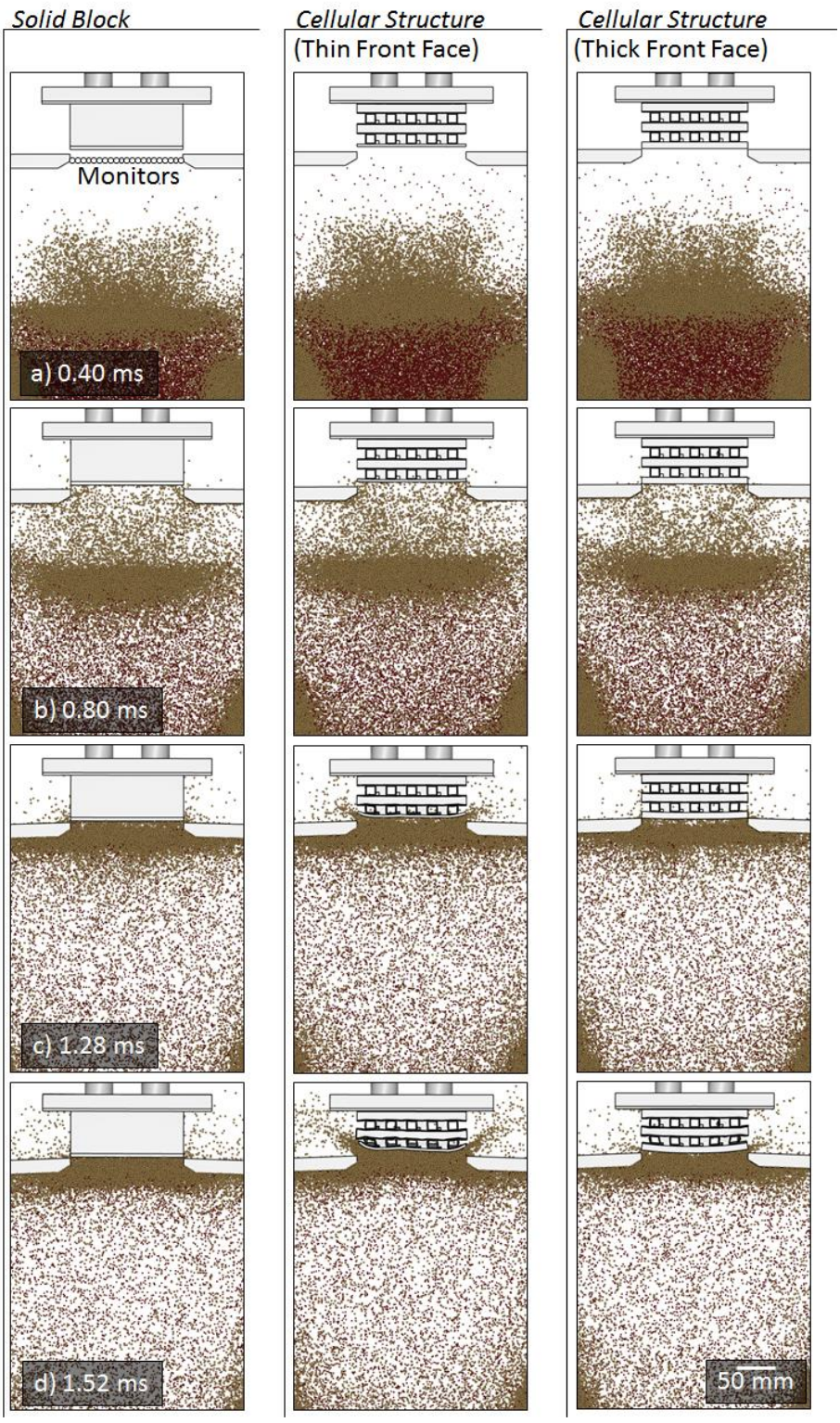

Figure 11. A sand particle propagation sequence for simulations with a solid block, a thin faced sandwich structure and a thick faced sandwich structure at a standoff distance of 40 cm.

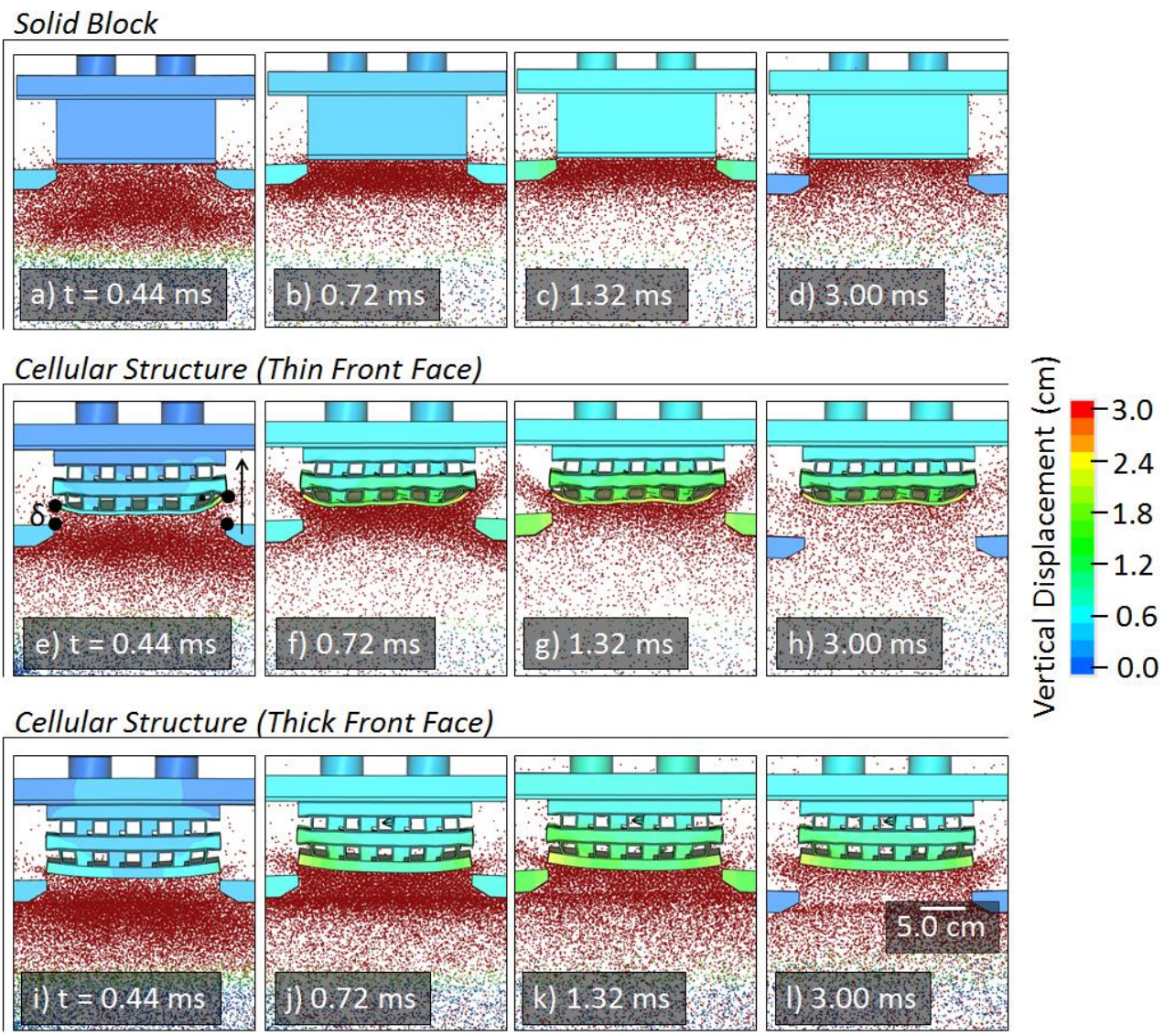

Figure 12. Detailed simulations show the vertical displacement of the solid block and two cellular test structures for a 14 cm standoff distance. The sand box lid vertical displacement during the sand particle loading process is also shown.

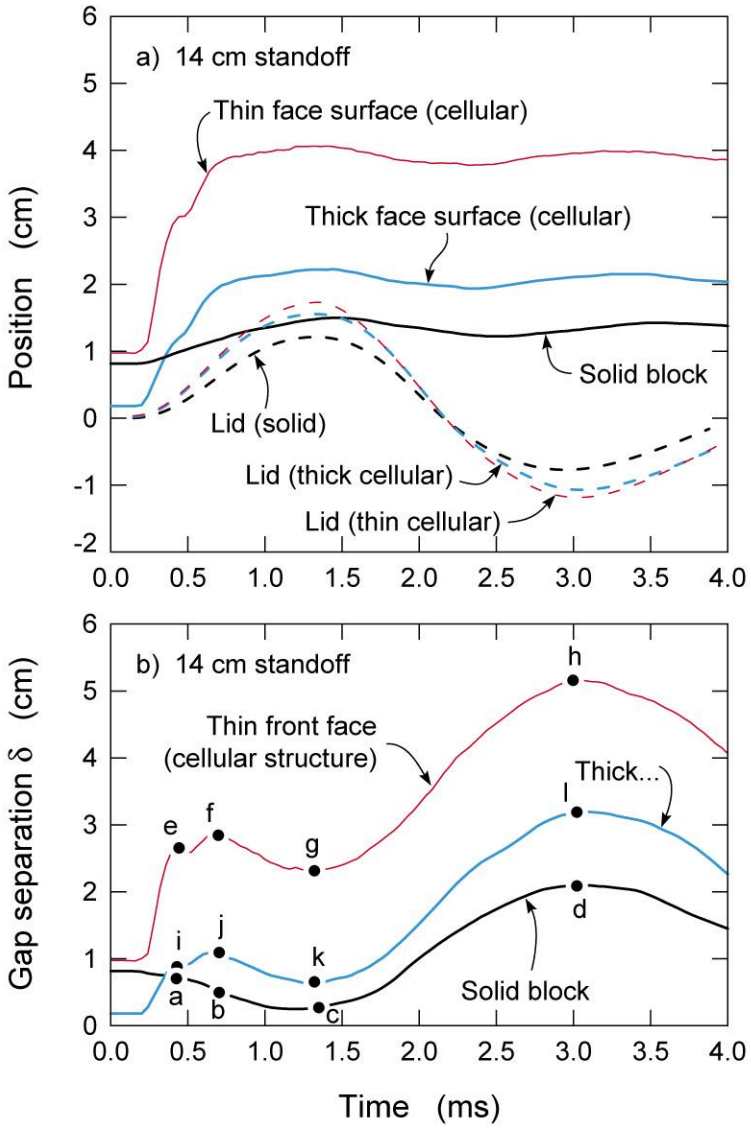

Figure 13. (a) The simulated position change of the steel lid was monitored (dashed lines) and compared to the monitored position at the surface of the solid block and thin and thick cellular structures (solid lines). (b) The simulated vertical gap separation between the lid and the surface of the three tested samples for the 14 cm standoff test. The lettered dots correspond to images shown by Figure 12.

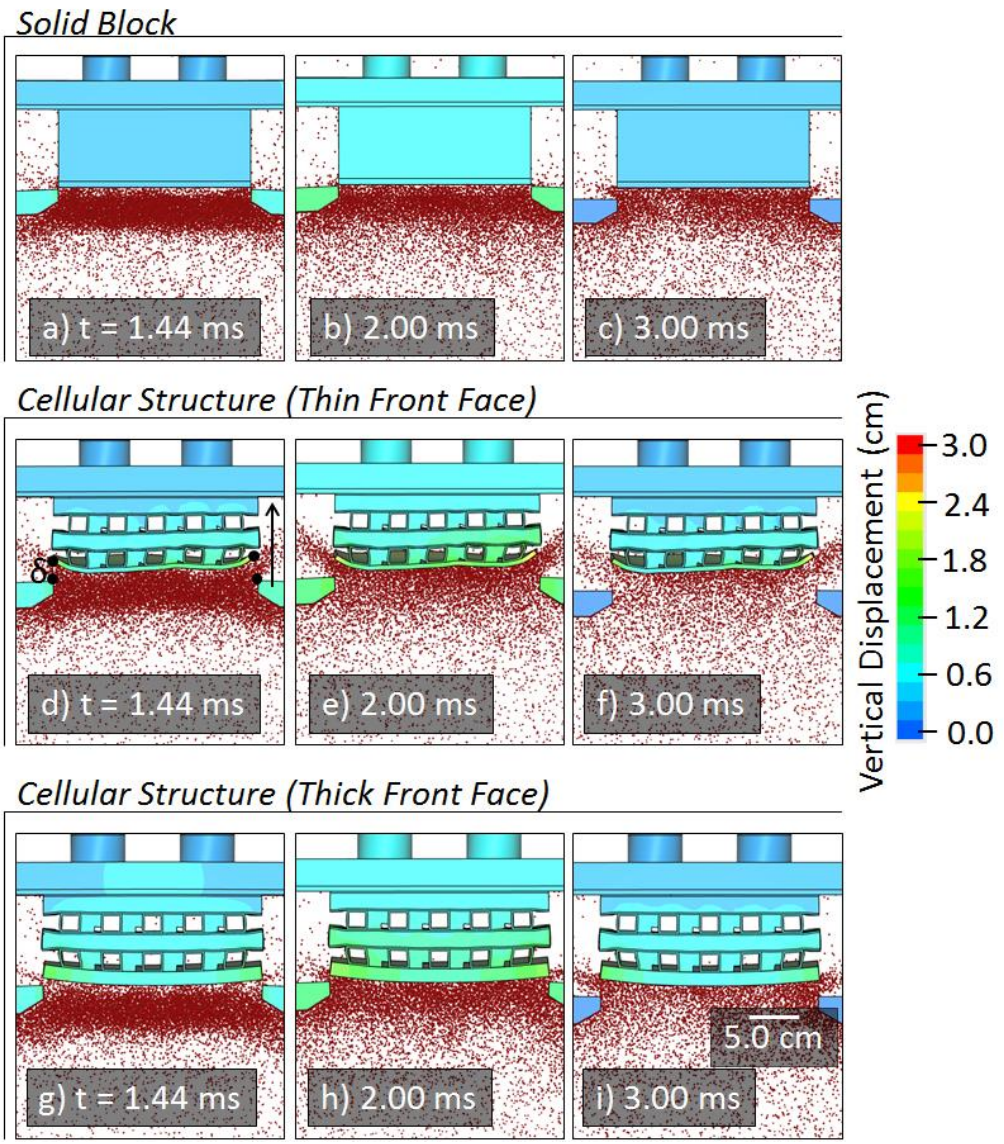

Figure 14. Detailed simulations show the vertical displacement of the solid block and two cellular test structures for a 40 cm standoff distance. The sand box lid vertical displacement during the sand particle loading process is also shown.

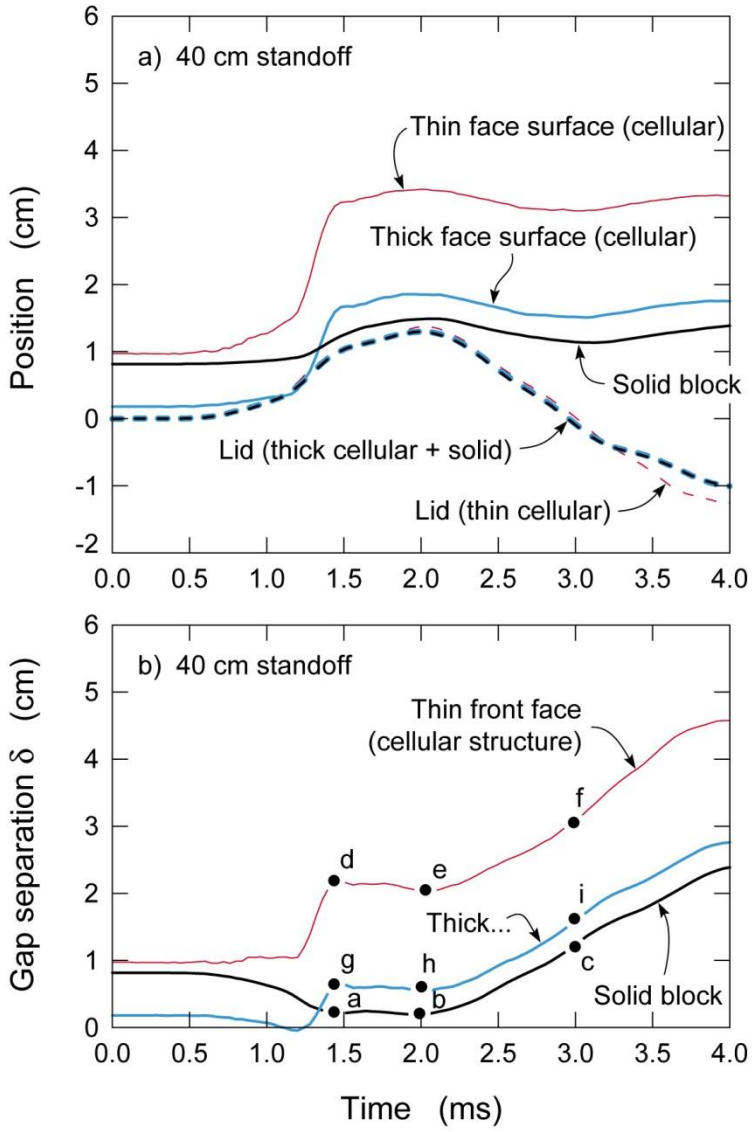

Figure 15. (a) The simulated position change of the steel lid was monitored (dashed lines) and compared to the monitored position at the surface of the solid block and thin and thick cellular structures (solid lines) at a 40 cm standoff. (b) The simulated vertical gap separation between the lid and the surface of the three tested samples for the 40 cm standoff test. The lettered dots correspond to images shown by Figure 14.

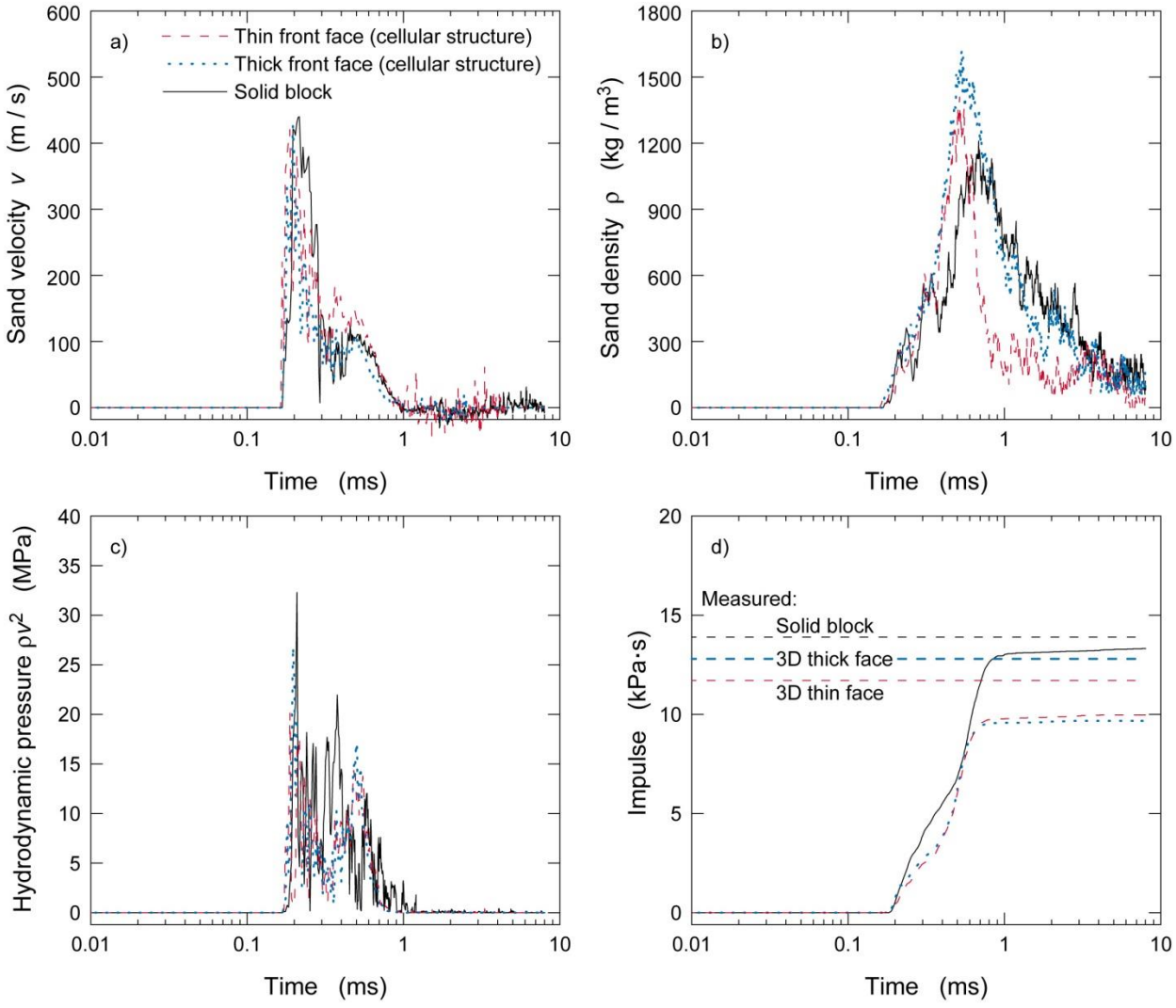

Figure 16. a) The sand velocity and b) sand density determined at monitors located 2.5 cm below the sample surface for a solid block (black), and thin (red) and thick (blue) faced sandwich structure for a standoff distance of 14 cm. The calculated hydrodynamic pressure c) and the sand impulse d) at the same monitor levels are also shown.

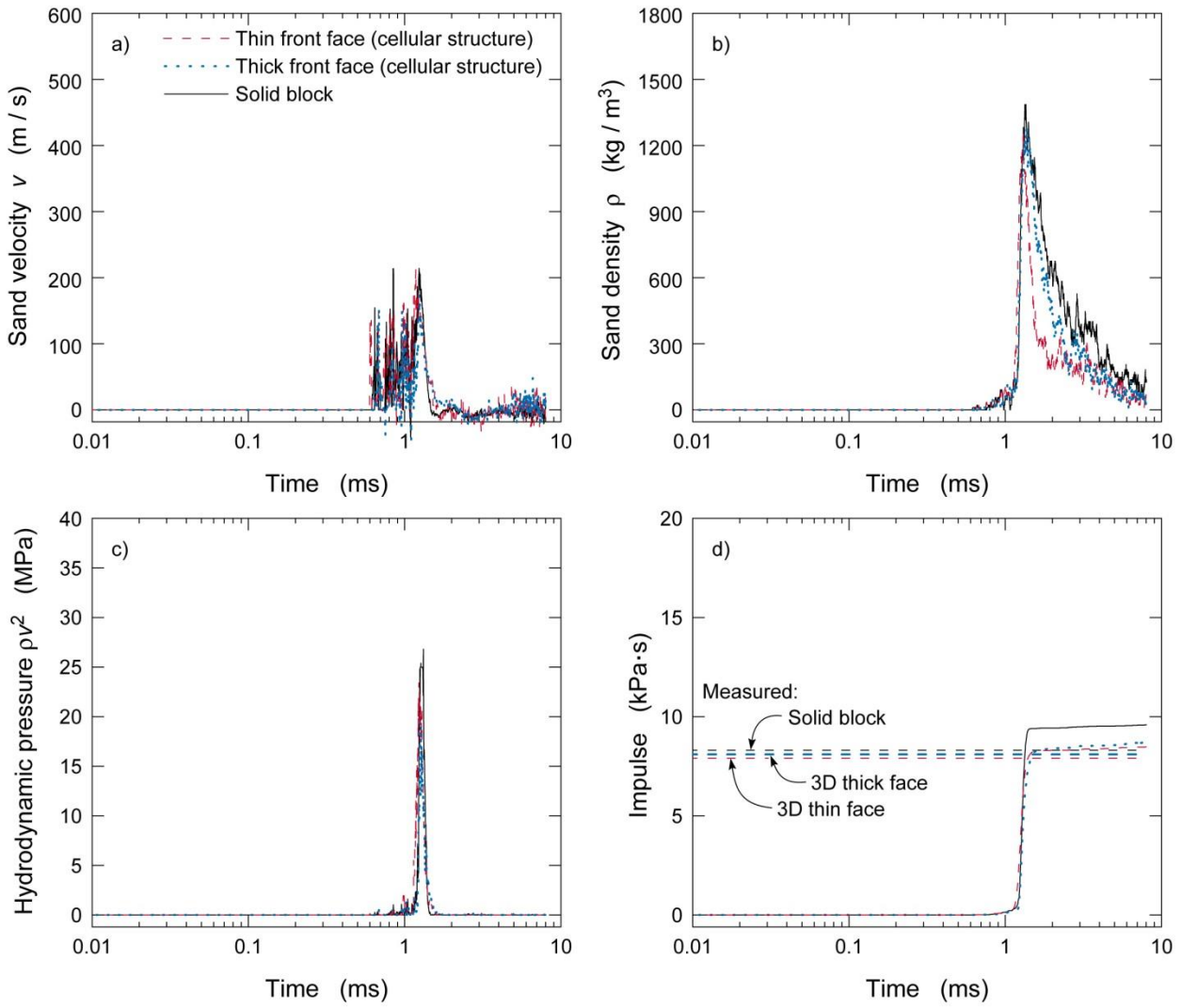

Figure 17. a) The sand velocity and b) sand density determined at monitors located 2.5 cm below the sample surface of a solid block (black), and thin (red) and thick (blue) faced sandwich structure for a standoff distance of 40 cm. The calculated hydrodynamic pressure c) and the sand impulse d) at the same monitor levels are also shown.

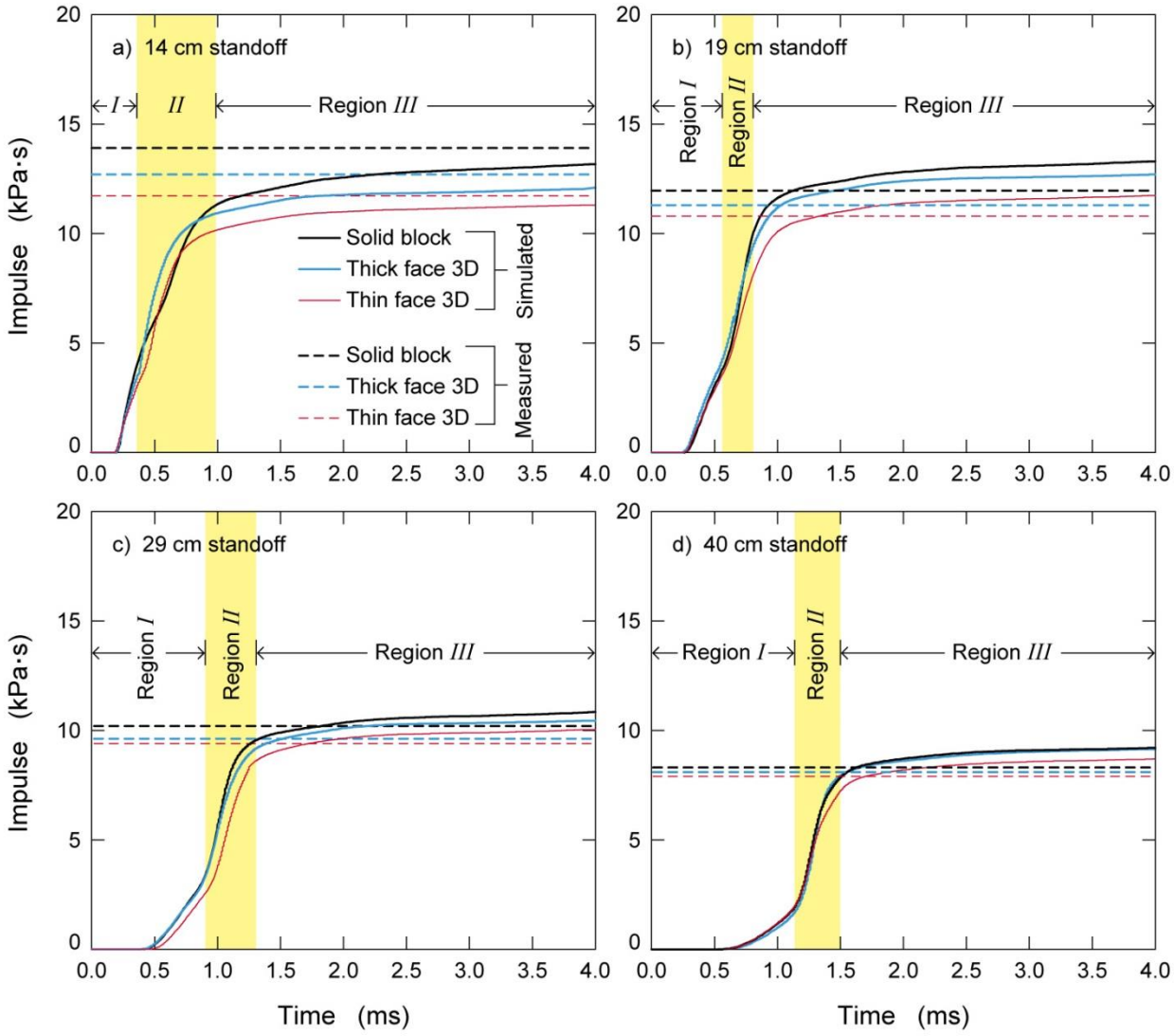

Figure 18. Simulated impulse-time responses determined from the sand particle contact with the front face of the solid block (black) and sandwich structures thin (red) and thick (blue) front faces for standoff distances of a) 14cm, b) 19cm, c) 29cand d) 40cm. The measured total impulse is shown as dashed lines whose colors correspond to those of the simulated structures.

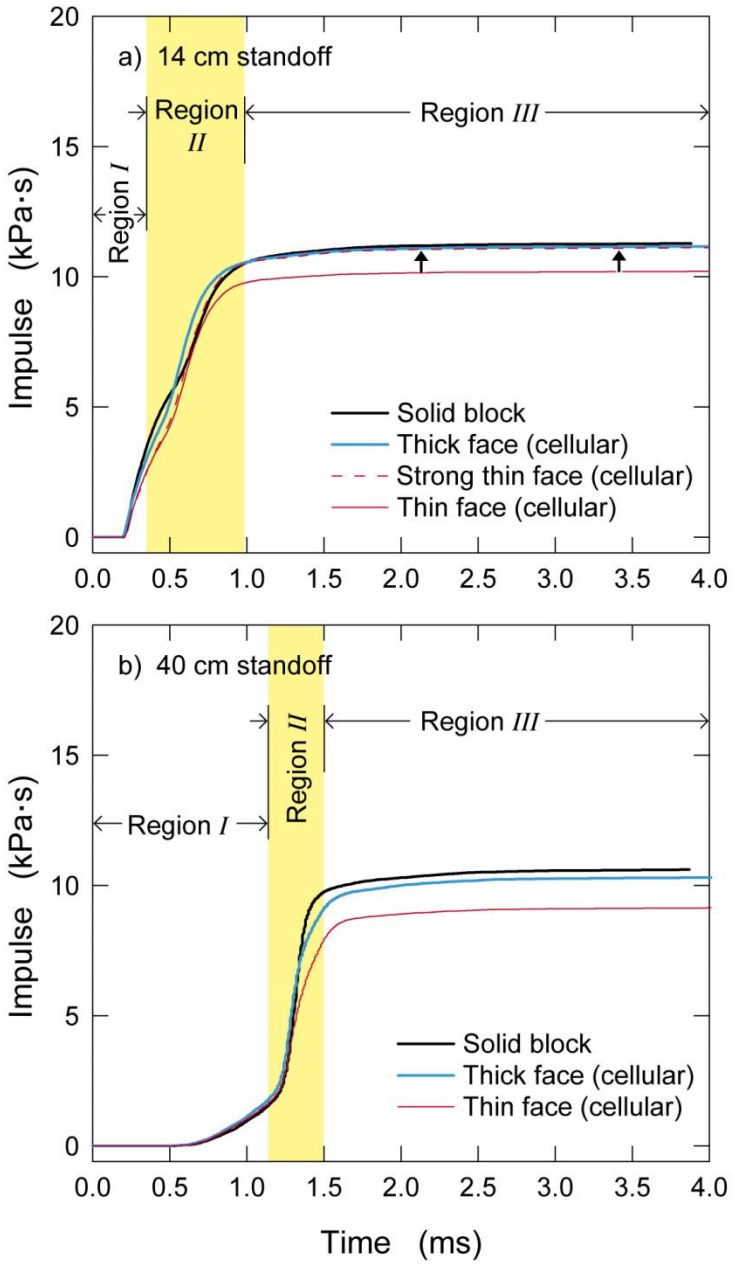

Figure 19. Simulated impulse-time responses determined from the sand particle contact with the front face of the solid block and thin and thick sandwich structures with no box top present for standoff distances of a) and d) 40cm.

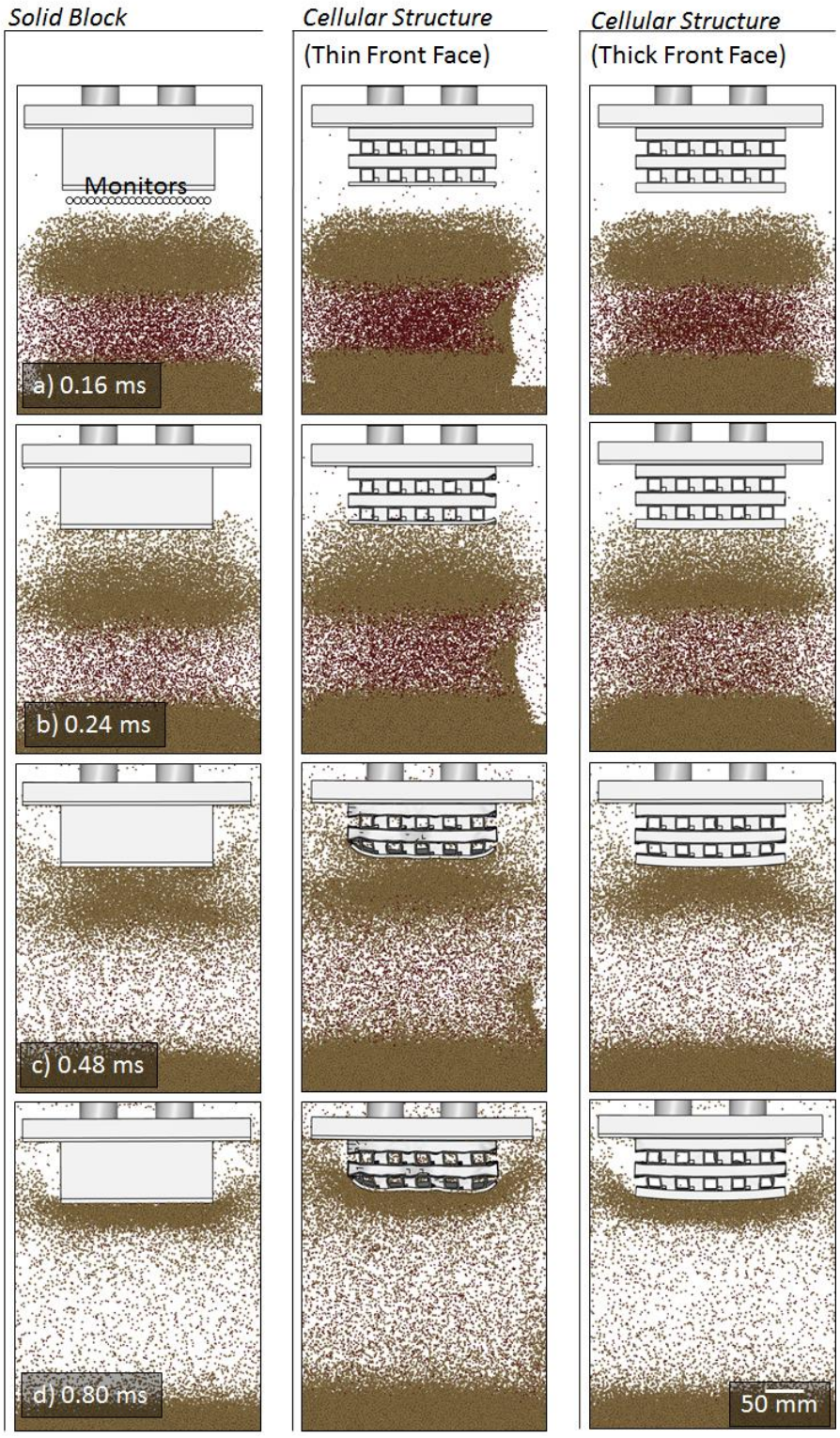

Figure 20. A sand particle propagation sequence for simulations with a solid block, a thin faced sandwich structure and a thick faced sandwich structure at a standoff distance of 14 cm with the box top removed. The red particles correspond to the explosive gases while the brown particles correspond to sand. Air particles are not shown.

Figure 21. A sand particle propagation sequence for simulations with a solid block, a thin faced sandwich structure and the thick faced sandwich structure at a standoff distance of 40 cm with the box top removed.

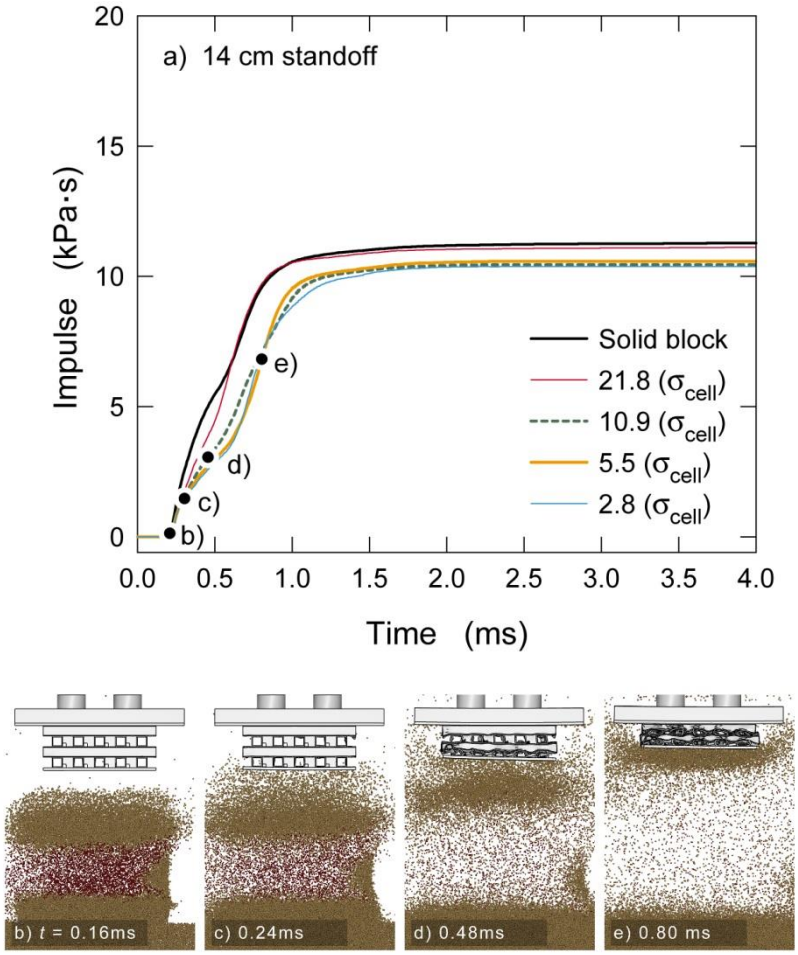

Figure. 22. a) Predicted transferred impulse-time responses at a 14 cm standoff distance without a box top lid for the solid block (black), and sandwich structures with a rigid thin front face and cellular cores of differeing strengths (red, green, orange and pink) whose compressive strengths are shown in units of MPa. (b-e) Show snap shots of the sand loading against the rigid thin face cellular structure with a core strength of 10.9 MPa (green curve in (a)).

Table 1. Core dimensions for back-supported test specimens with 4.7 and 12.7 mm thick impact faces.

Sample	In-plane tube wall thickness, t (mm)	In-plane tube width, l (mm)	Out-of-plane tube wall thickness, t_v (mm)	Out-of-plane tube width, l_v (mm)	face sheet thickness, t_{fs} (mm)	Specimen weight (kg)	Core weight (kg)	Relative density (%)
3D (4.7 mm)	1.45	19.05	1.45	19.05	4.7	3.22	1.51	20.1
3D (12.7 mm)	1.45	19.05	1.45	19.05	12.7	4.03	1.51	20.1

Table 2. Transmitted impulse for solid sample and cellular test specimens with 4.7 and 12.7 mm thick impact face sheet thicknesses

Sample	*Standoff Distance (cm)*	*Charge Mass (C4 Insert Mass) (g)*	*Average Core Strain, ε_c (%)*	*Mass of Pendulum with Sample and Counterweights (kg)*	*Jump Height, h_{max}, (m)*	*Transferred Impulse ($kPa \cdot s$)*
Solid	14	300 (50)	_	106.6±0.15	1.49±0.17	13.9±0.8
3D (12.7mm)			18.6	106.3±0.15	1.22±0.15	12.6±0.8
3D (4.7mm)			20.1	106.9±0.15	1.05±0.16	11.7±0.9
Solid	19	300 (50)	_	92.3±0.15	1.46±0.21	12.0±0.9
3D (12.7mm)			14.5	92.0±0.15	1.31±0.17	11.3±0.8
3D (4.7mm)			18.1	92.7±0.15	1.18±0.19	10.8±0.9
Solid	29	300 (50)	_	85.1±0.15	1.26±0.24	10.2±1.0
3D (12.7mm)			6.8	85.4±0.15	1.11±0.17	9.6±0.8
3D (4.7mm)			8.9	85.3±0.15	1.05±0.21	9.4±1.0
Solid	40	300 (50)	_	85.1±0.15	0.84±0.17	8.3±0.8
3D (12.7mm)			3.2	85.4±0.15	0.78±0.15	8.1±0.8
3D (4.7mm)			3.4	85.3±0.15	0.69±0.13	7.9±0.7

Table 3. Transmitted pressures for samples with 4.7 mm thick face sheets determined with Hopkinson pressure bars.

Sample	*Standoff Distance (cm)*	*Average Core Strain, ε_c (%)*	*Peak Pressure (MPa)*	*Transferred Impulse at 558μs, I, (kPa-s)*	*$\frac{dI}{dt} = \dot{I}$ (MPa)*
Solid	14	_	28.2	10.8	21.5
3D cellular		20.1	19.4	7.9	18.8
Solid	19	_	25.3	8.9	18.0
3D cellular		18.1	17.8	7.0	16.0
Solid	29	_	14.2	6.4	11.4
3D cellular		8.9	12.2	5.1	11.2
Solid	40	_	9.3	4.6	8.1
3D cellular		3.4	7.2	2.9	6.9

Table 4. Material yield and cellular compressive strength, and impulse transfer rate and maximum transmitted pressure

Sample	*Material Yield Strength (MPa)*	*Compressive Strength (MPa)*	*Impulse rate (MPa)*
Solid Block	350.0	-	20.7
3D cellular	230.7	21.8	13.7
3D cellular	115.4	10.9	7.9
3D cellular	57.7	5.5	6.9
3D cellular	28.8	2.5	6.4